Asia-Pacific School and Workshop on Gravitation and Cosmology 2020

Lecture 2
Gravitational Waves: Astrophysics
중력파: 천체물리학

Alex Nielsen (유진)
University of Stavanger

Hulse–Taylor Radio Pulsar PSR1913+16 (1974)

Source : NSF

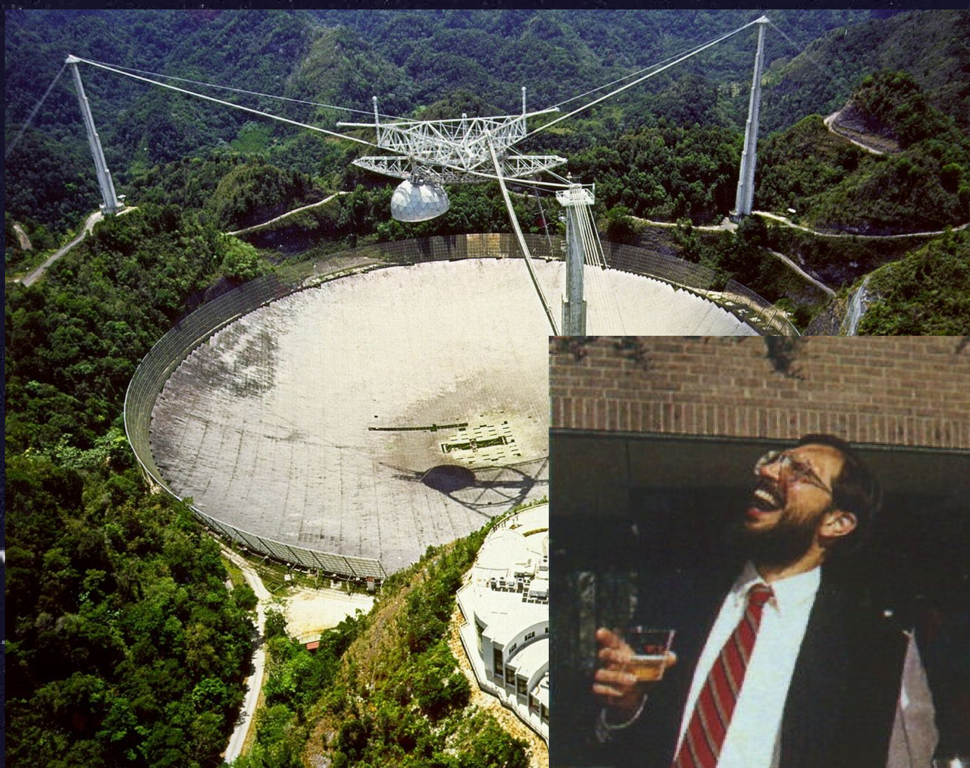

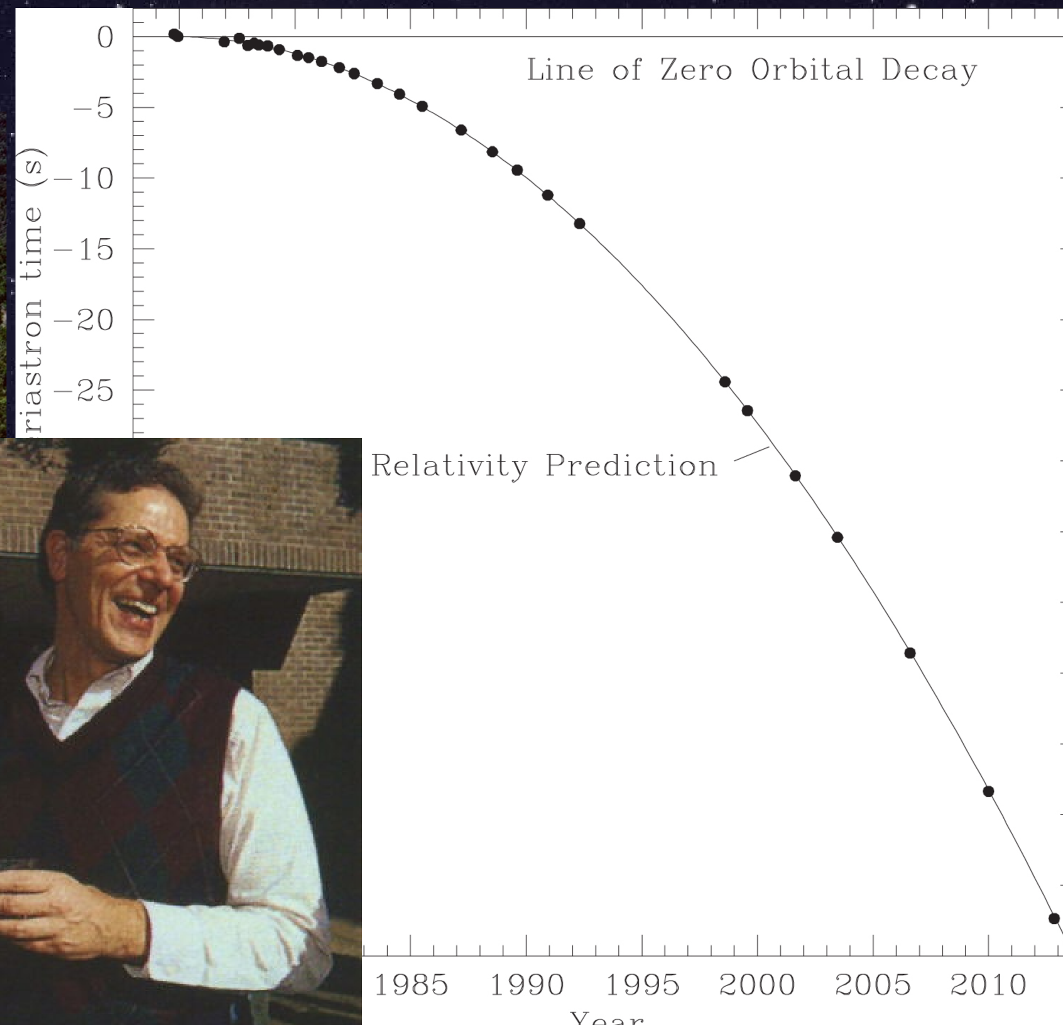

Weisberg and Huang ApJ 829 (2016) 55

Nobel Prize 1993

Mathematical doubts persist...

The Astrophysical Journal, 208:L77–L81, 1976 September 1

COMMENTS ON GRAVITATIONAL RADIATION DAMPING AND ENERGY LOSS IN BINARY SYSTEMS

Jürgen Ehlers and Arnold Rosenblum
Max-Planck-Institut für Physik und Astrophysik, Munich, Germany

Joshua N. Goldberg
Department of Physics, Syracuse University

and

Peter Havas
Department of Physics, Temple University
Received 1976 April 12; revised 1976 June 21

ABSTRACT

It is argued that a formula for the energy loss due to gravitational radiation of bound systems such as binaries has not yet been derived either exactly or by means of a consistent approximation method within general relativity, a view which contradicts some widely accepted claims in the literature. The main approaches used to obtain such a formula are critically reviewed, and it is pointed out that the derivations presented so far either contain inconsistencies or are incomplete.
Subject headings: gravitation — relativity — stars: binaries

The determination of radiation reaction forces is a fundamental problem of any field theory of gravitation. More specifically, the discovery of the binary pulsar PSR 1913+16 and systems such as Ariel 1118−61 has concerned here not with a field theory of gravitation in the abstract, but with a particular one: Einstein's general theory of relativity. While in some respects Einstein's theory indeed has the same structure and

Propagation of gravitational waves

Plasma mean free path: $L = \frac{1}{n\sigma} \approx \frac{c^4}{nG^2 m_p^2} \approx (10^{110})m$

"...any reasonable regularization of the vacuum expectation value of the energy momentum tensor of the field must vanish. This means that a gravitational wave far from its source will propagate without hindrance by quantum effects."

Gibbons, Commun. Math. Phys 45 (1975) 191

$\langle 0|T_{ab}|0\rangle = 0$

2017 Nobel Prize in Physics

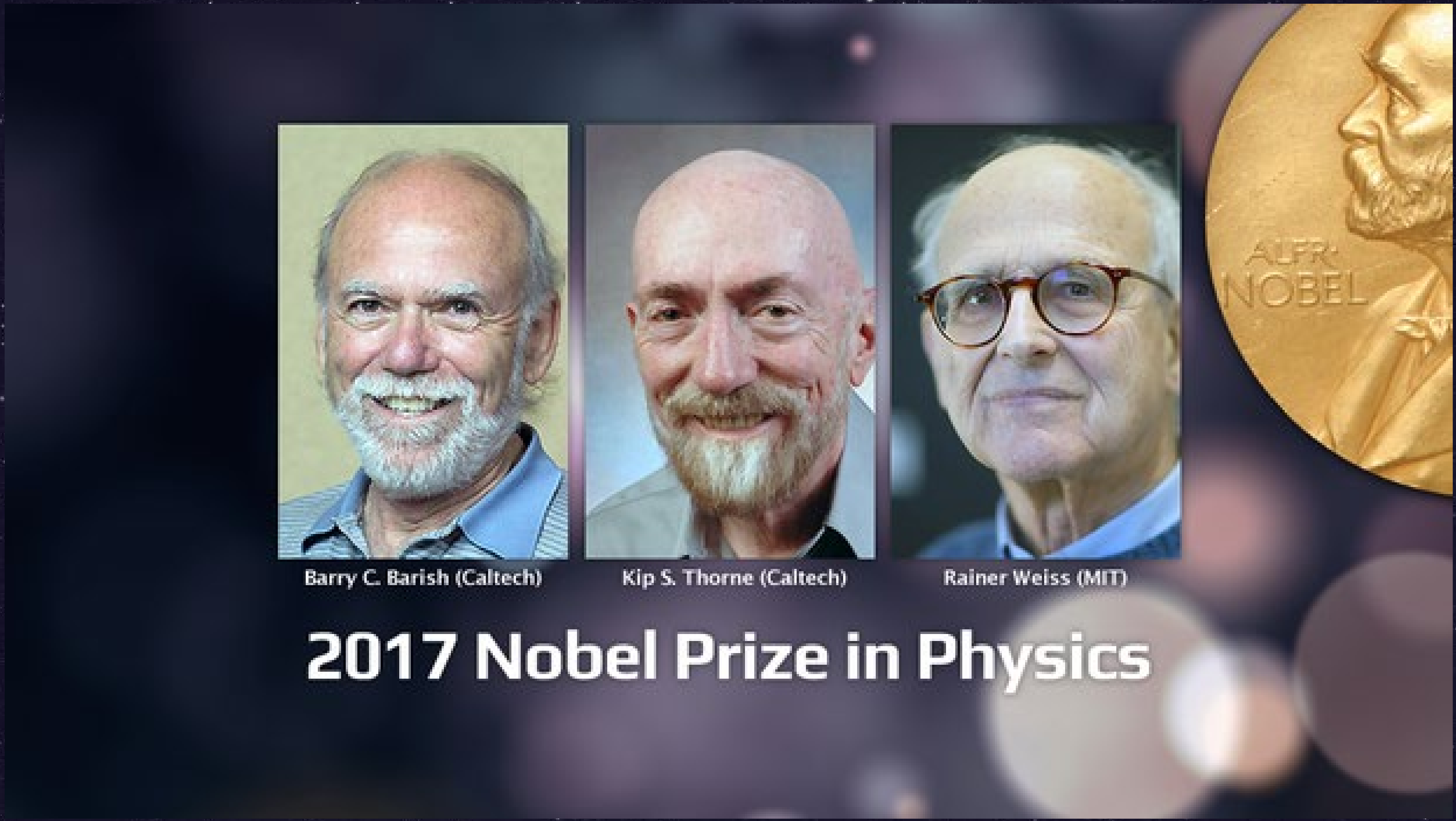

“"for decisive contributions to the LIGO detector and the observation of gravitational waves"”

USD 620 million*

Image source: otherhand.org
* Nature, 16 July 2014

Interferometers

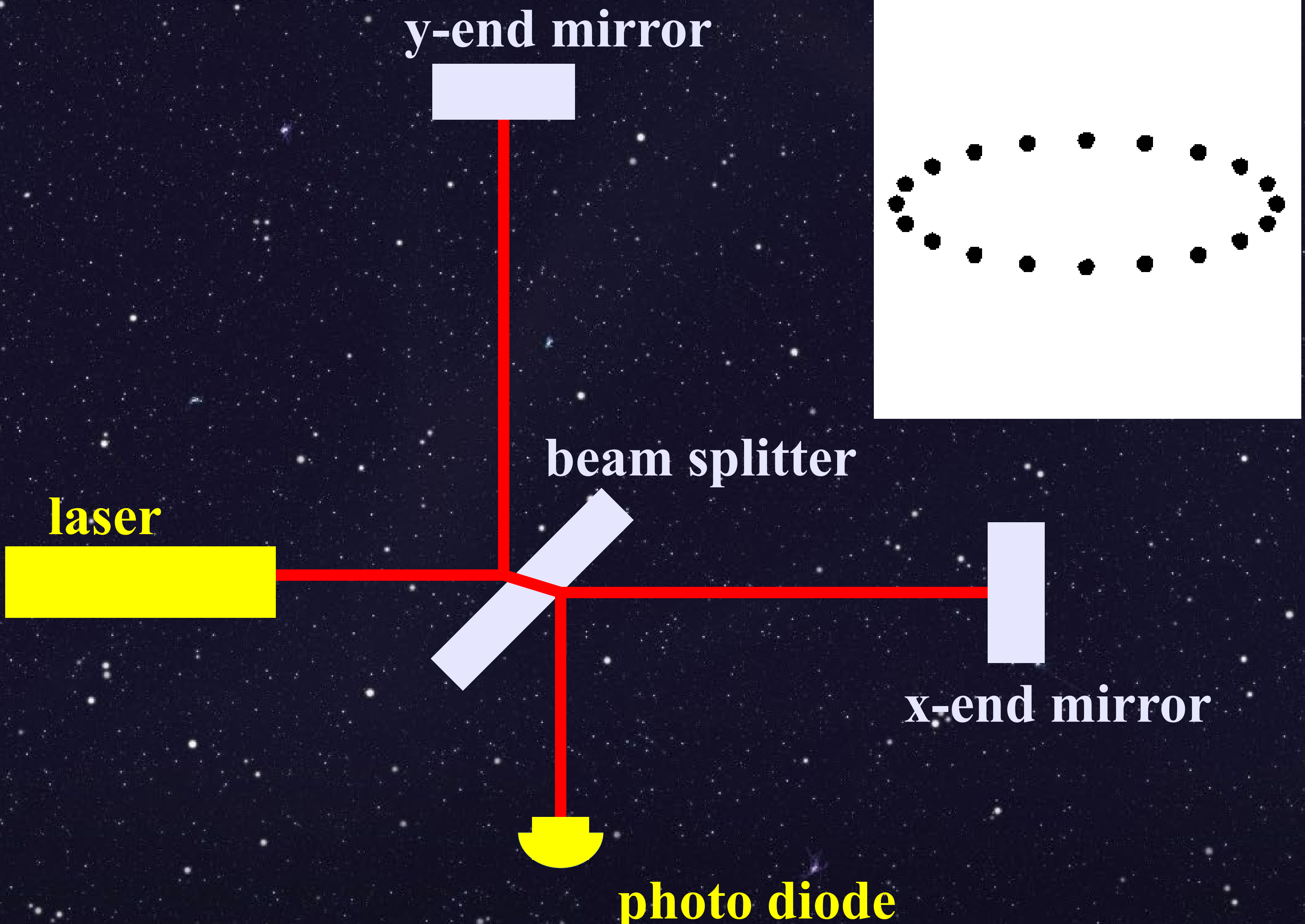

Reading between the lines

Interference pattern: $P_{out} = P_{max}\cos^2\Delta\phi$

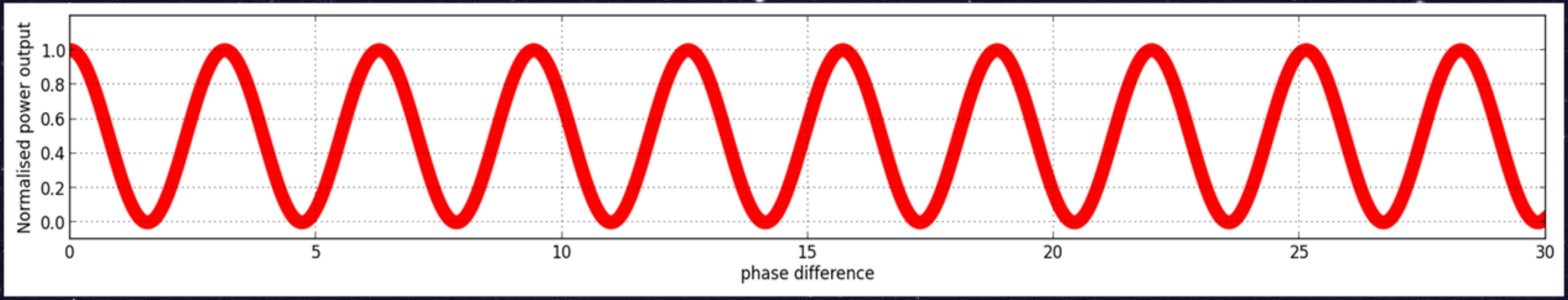

$$\Delta\phi = \frac{\pi}{2} + B\frac{c\Delta T}{\lambda}$$:Accumulated phase difference

Displacement sensitivity: $\Delta L = \frac{\lambda}{B}\sqrt{\frac{P_{out}}{P_{max}}}$

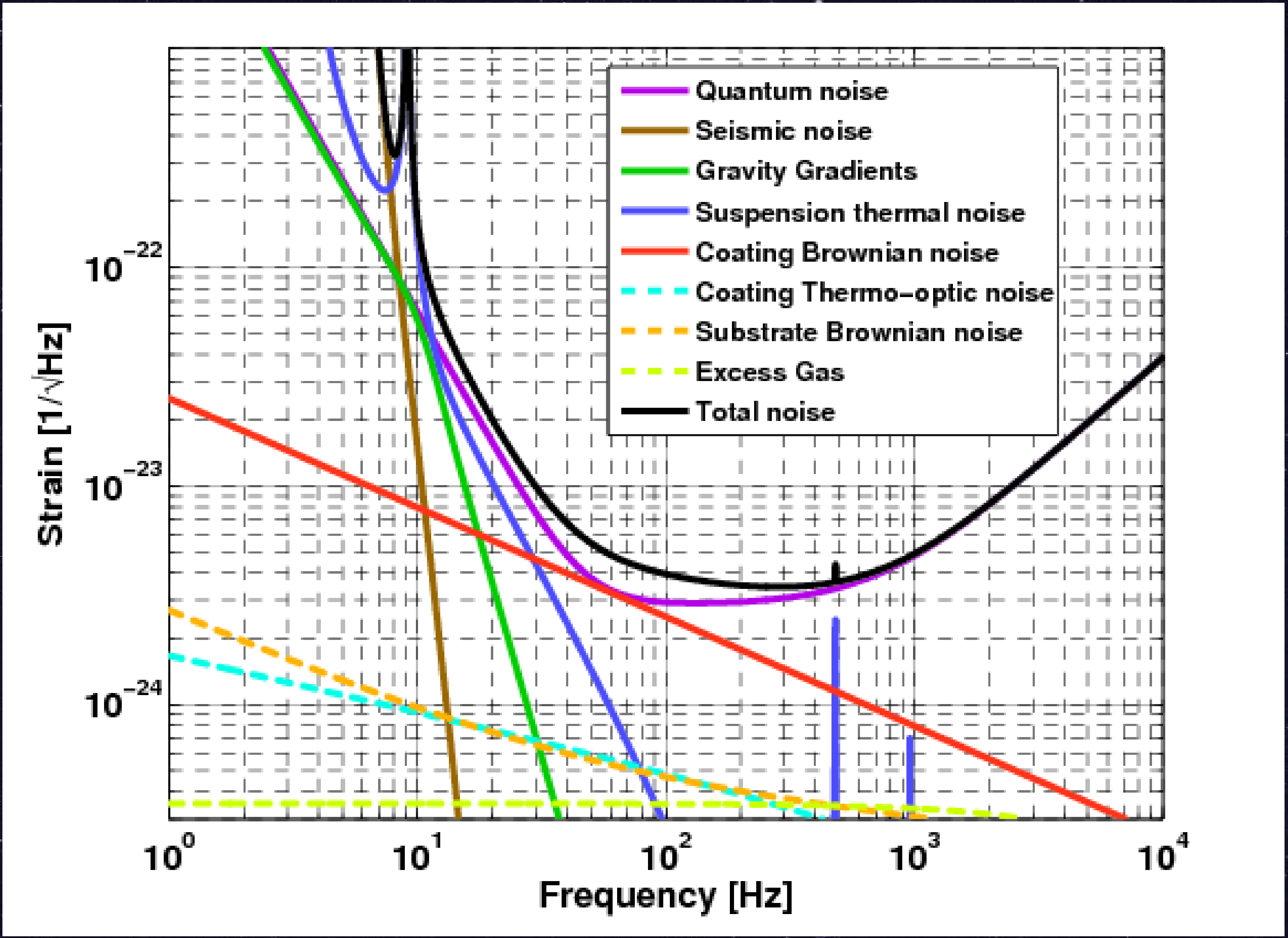

Source: *S. Hild (2012)*

Spectral lines

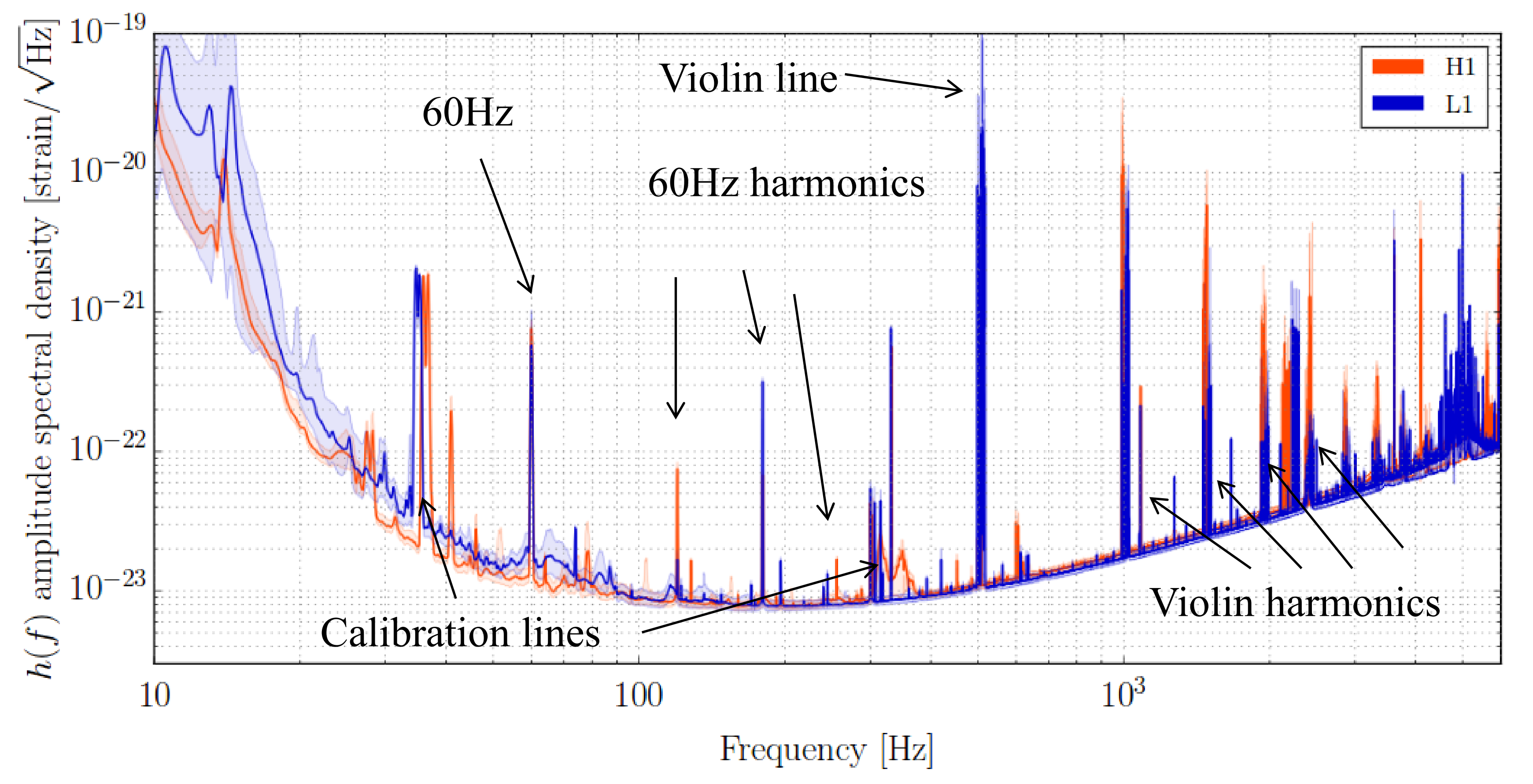

Fig. 1 Abbott et al. CQG33 (2016) 134001

aLIGO PEM SENSOR LOCATIONS: LHO

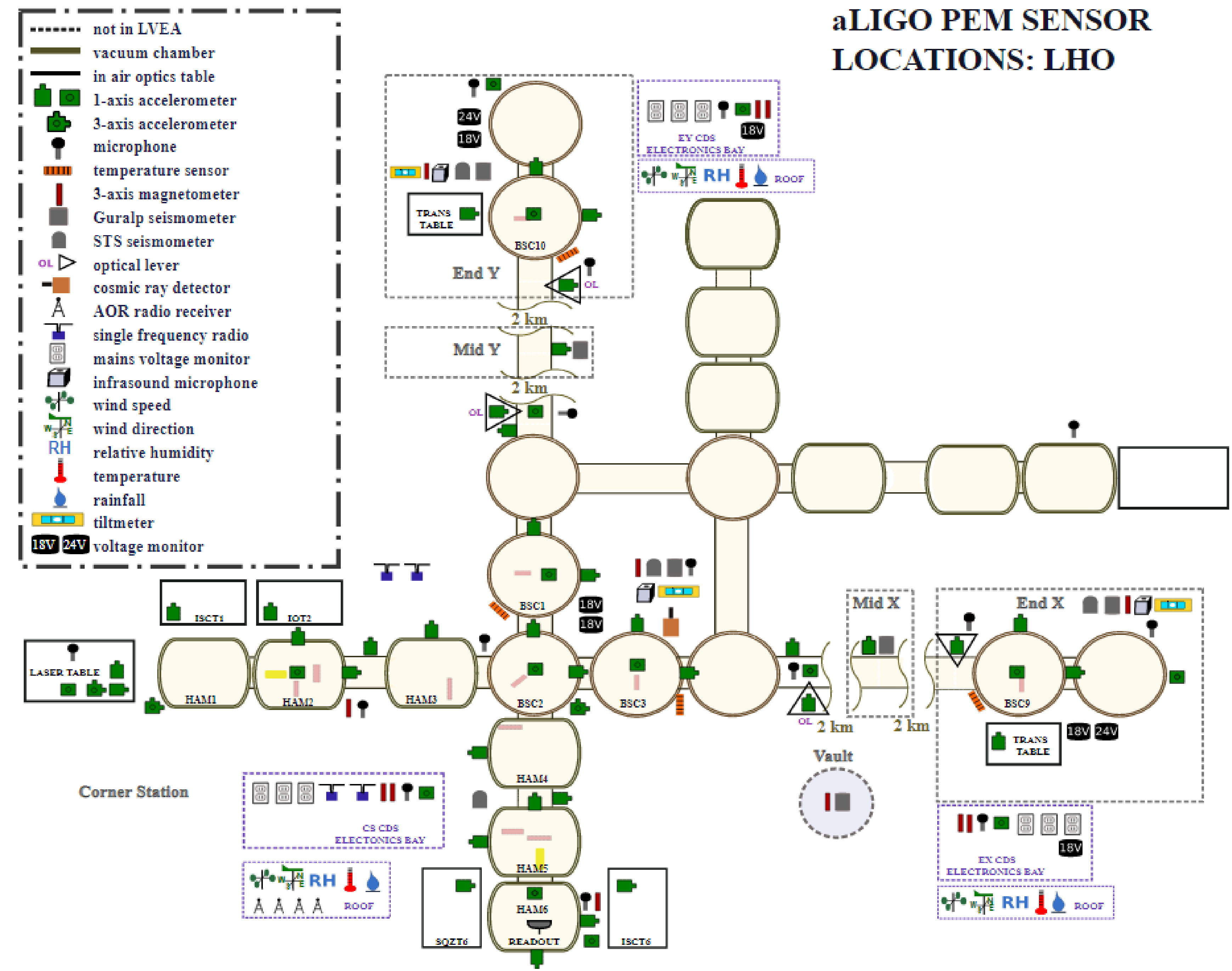

Source: ligo.pem.org

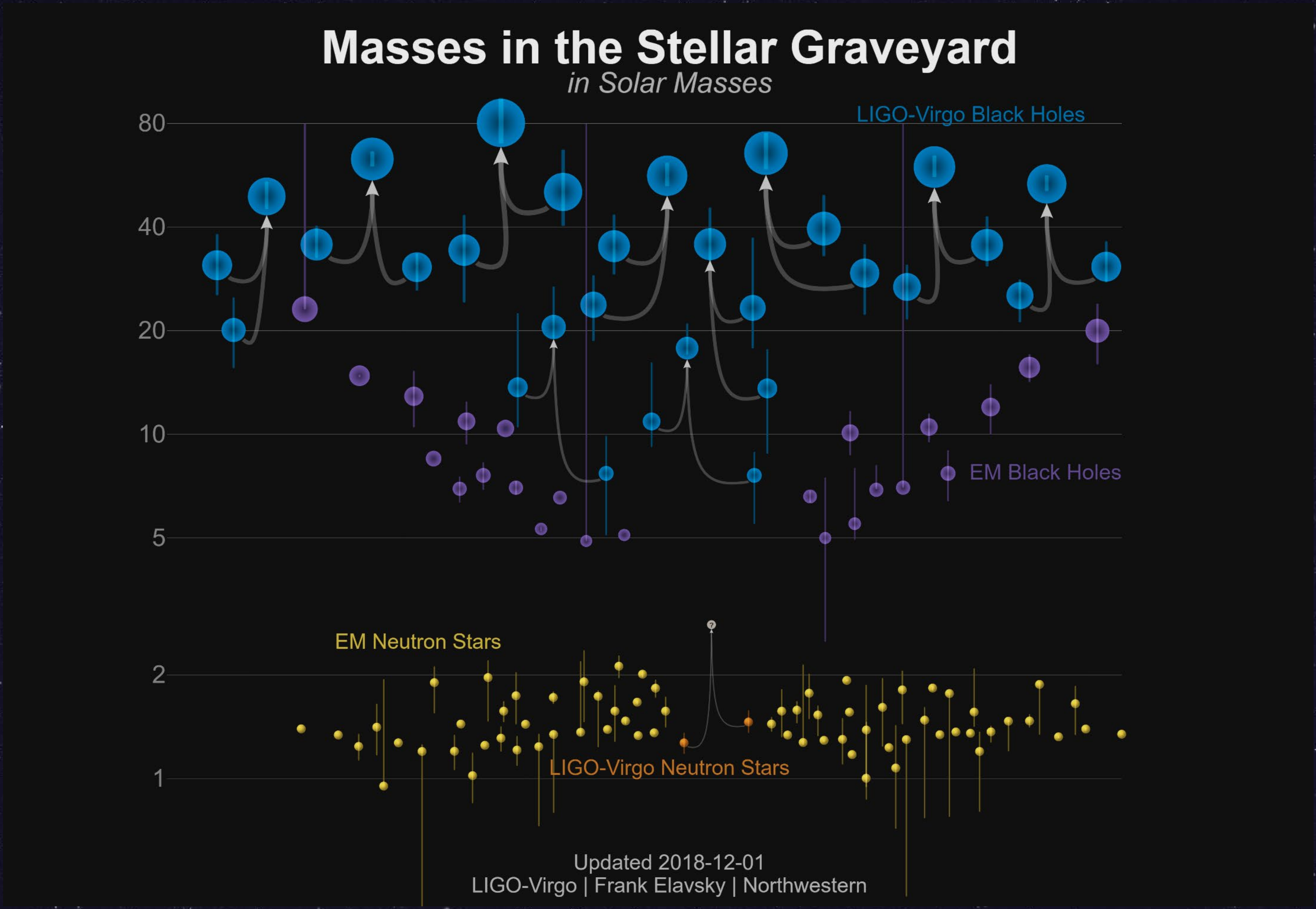

[Image credit: LIGO-Virgo/Frank Elavsky/Northwestern University]

Detection statistics

- **Task:** Separate data x into signals and noise
- **Approach:** Compute some statistic f(x) and compare to a threshold T.
- Neyman-Pearson criterion: maximise p(Detection) at fixed p(False alarm)
- **Solution:** compute a likelihood ratio

$$f(x) = \frac{p(x|H_{signal})}{p(x|H_{noise})} > T$$

Neyman, Pearson 1933

Bayesian interpretation

$$\frac{p(H_{signal}|x)}{p(H_{noise}|x)} = \frac{p(x|H_{signal})}{p(x|H_{noise})}\frac{p(H_{signal})}{p(H_{noise})}$$

$$p(x|H_{signal}) = \int p\,(x|\sigma, H_{signal})p(\sigma)d\sigma$$

Monte-Carlo simulation parameter distribution corresponds to prior parameter distribution

Searle 2008

Limitations in real life

- Need a parameterised noise model
- GW detectors: cannot turn off signal
- Need a parameterised signal model
- GW detectors: cannot turn on signal
- For large parameter spaces, marginalisation may be expensive
- Result will depend on prior distributions

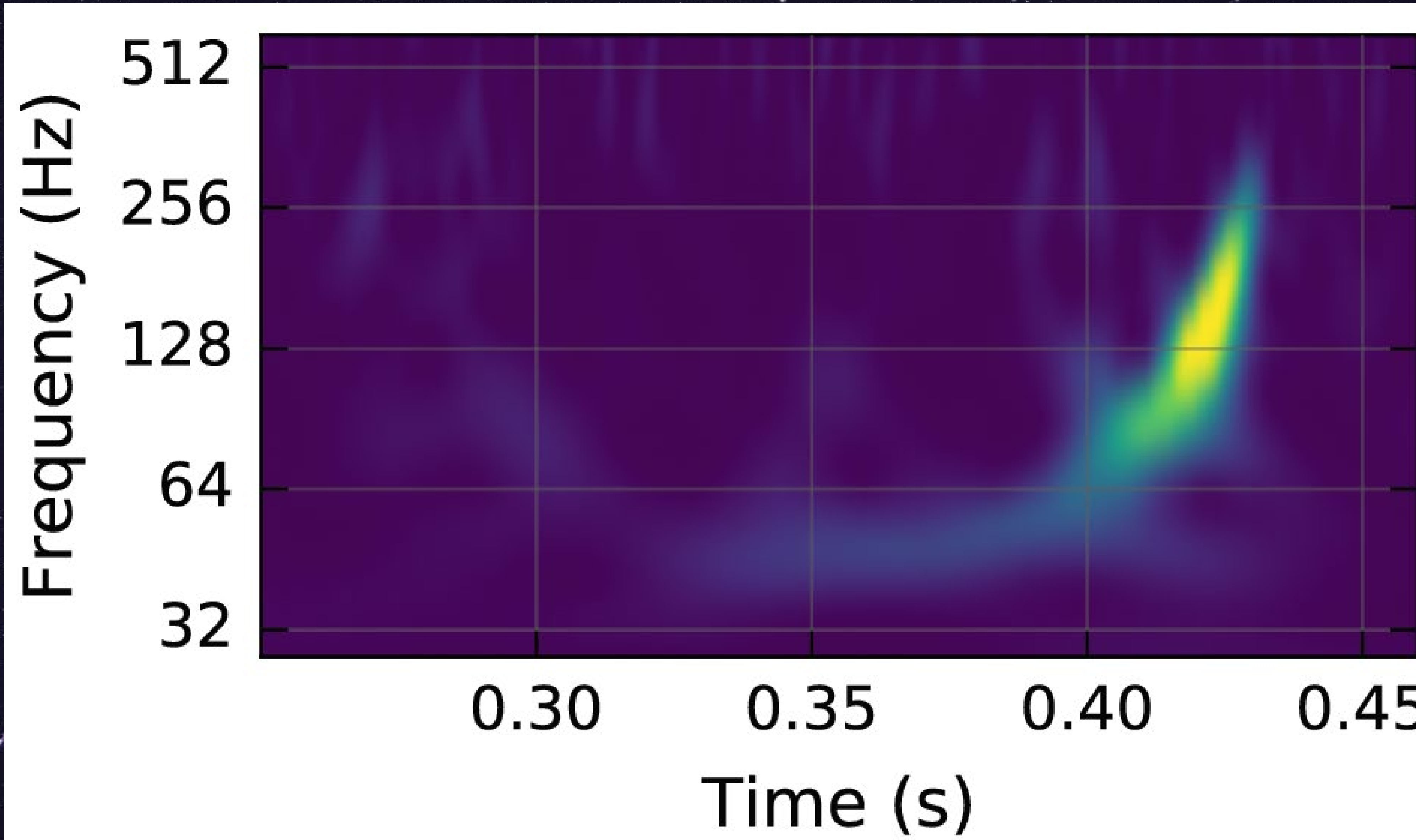

Part of Fig 1 of LVC, PRL116 (2016) 061102

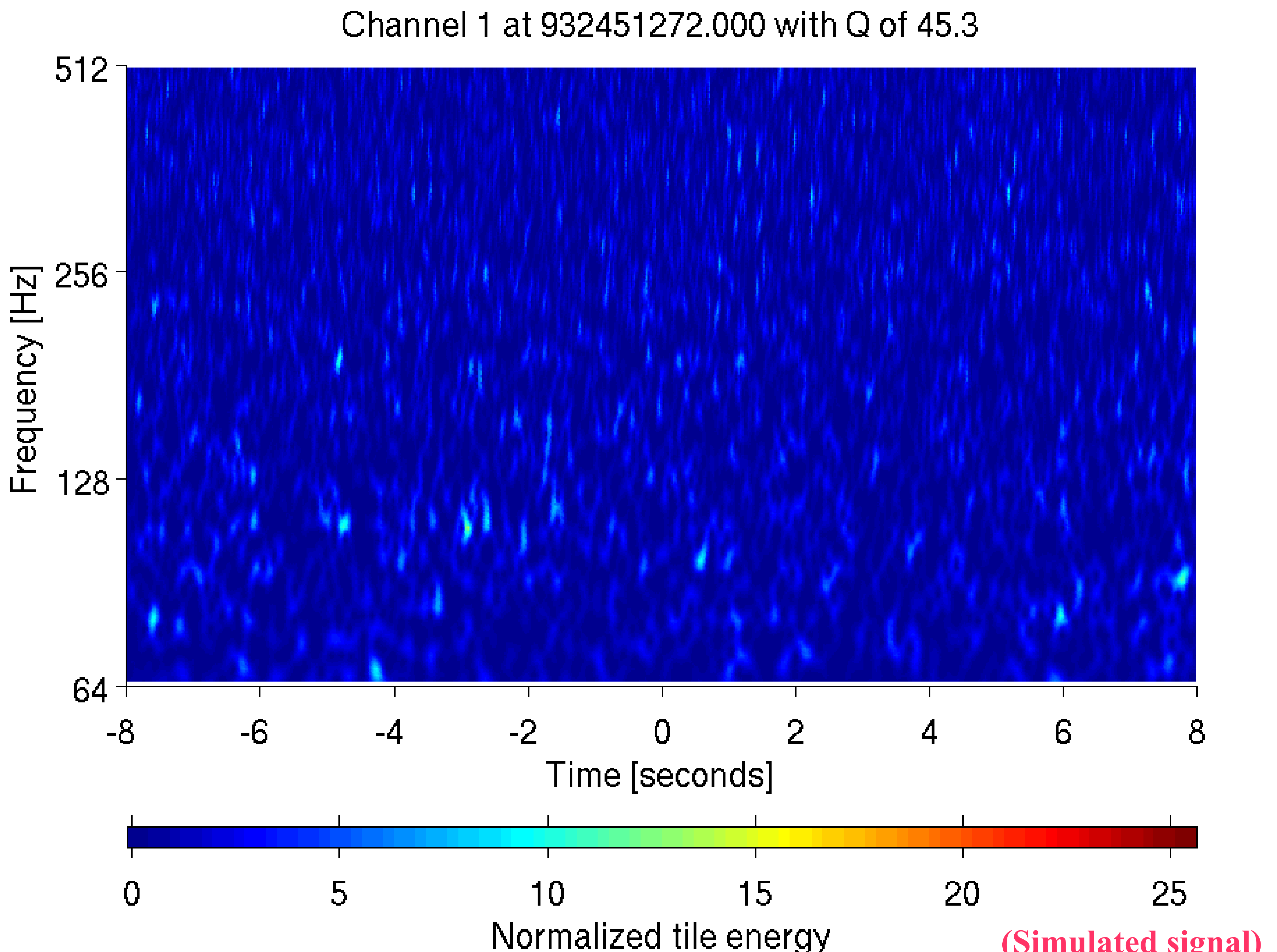

Channel 1 at 932451272.000 with Q of 45.3
Frequency [Hz]
512
256
128
64
-8
-6
-4
-2
0
2
4
6
8
Time [seconds]
0
5
10
15
20
25
Normalized tile energy
(Simulated signal)

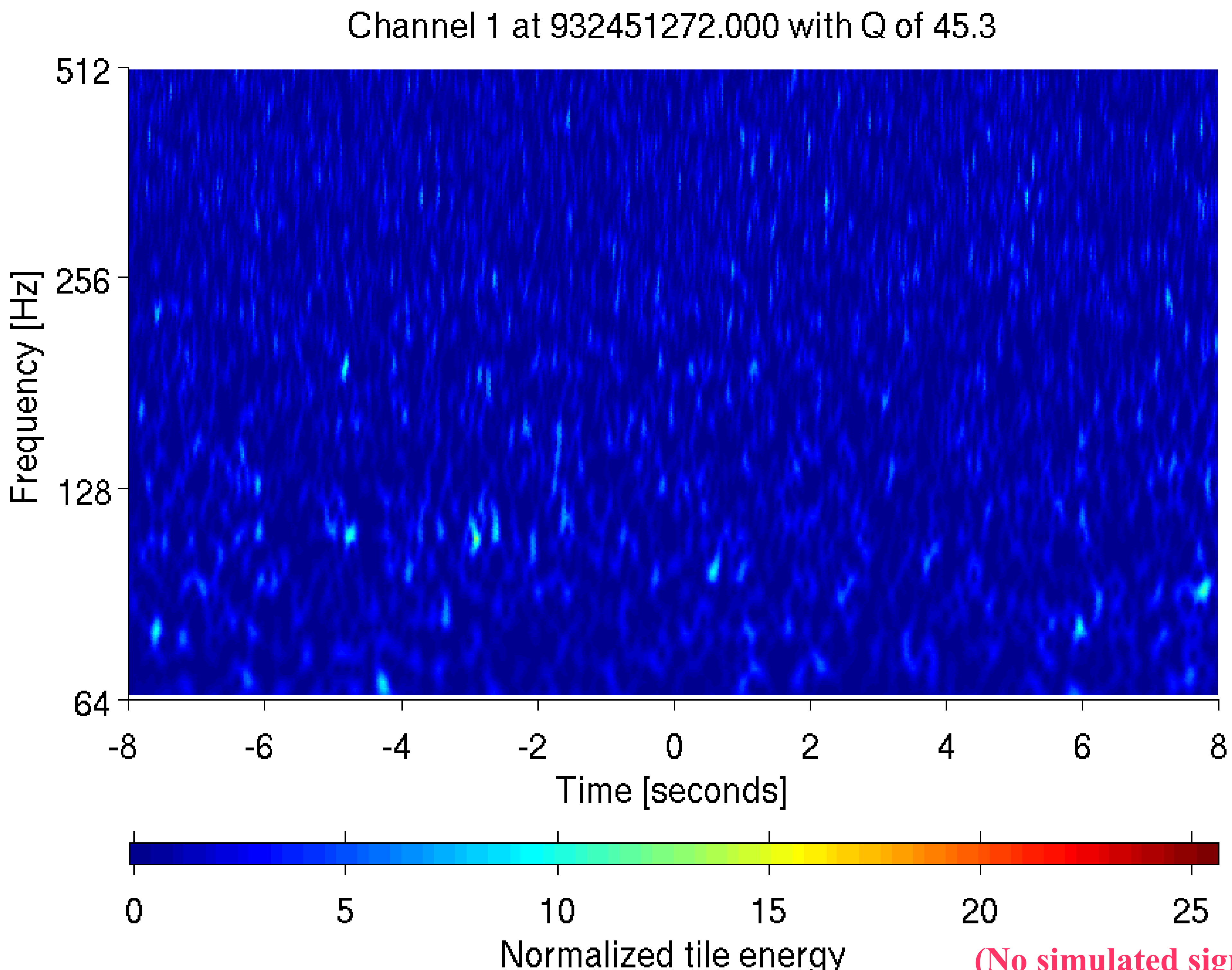

(No simulated signal)

Gravitational Waveforms

. Numerical relativity

either finite differencing or spectral methods

. Effective One Body (EOBNR)

maps two body problem to one body problem via effective Hamiltonian and calibrated to numerical simulations

. IMRPhenom

combines post-Newtonian inspiral with phenomenological fit model of numerical simulations of late inspiral and merger, and quasi-analytical ringdown phase

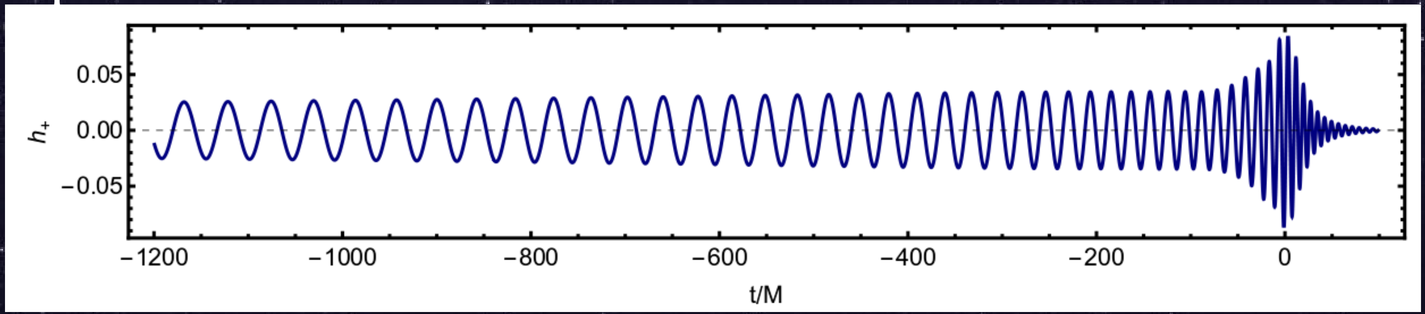

Source: Khan et al. PRD 93 (2016) 044007

Post-Newtonian expansion (2-2 phase)

PN order	Includes (amongst other things)
0PN	Kepler Newtonian Gravity
0.5PN	Zero in GR
1PN	Pericenter advance (cf zero) PPN parameters γ, β, ξ
1.5PN	Spin-orbit couplings Gravitational tails (backscatter)
2PN	Spin-spin couplings (Newtonian) quadrupole-monopole (GR BH) (Newtonian) magnetic dipole-dipole (cf zero)
3PN	Tails of tails
5PN	(Newtonian) Adiabatic tidal deformations

Fig 4 of LVC, PRL116 (2016) 061102

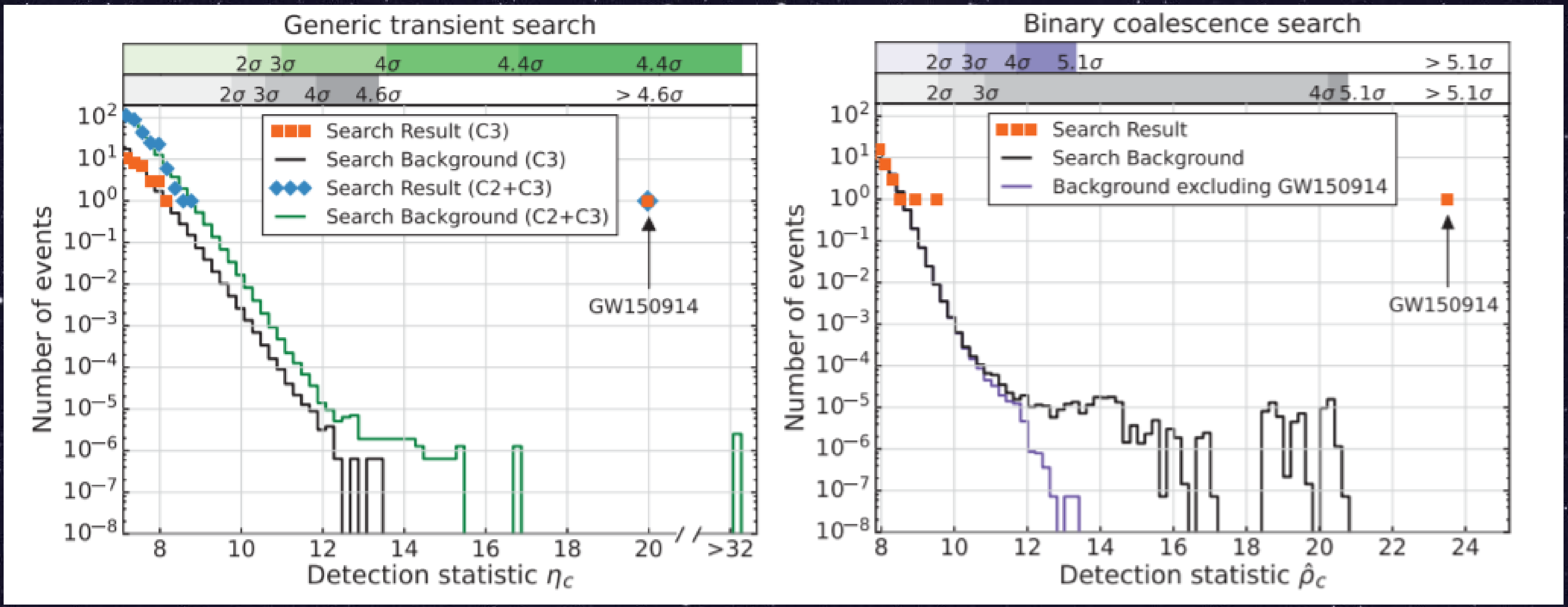

Unmodeled, coherent power search

Modeled, template-based matched filter search

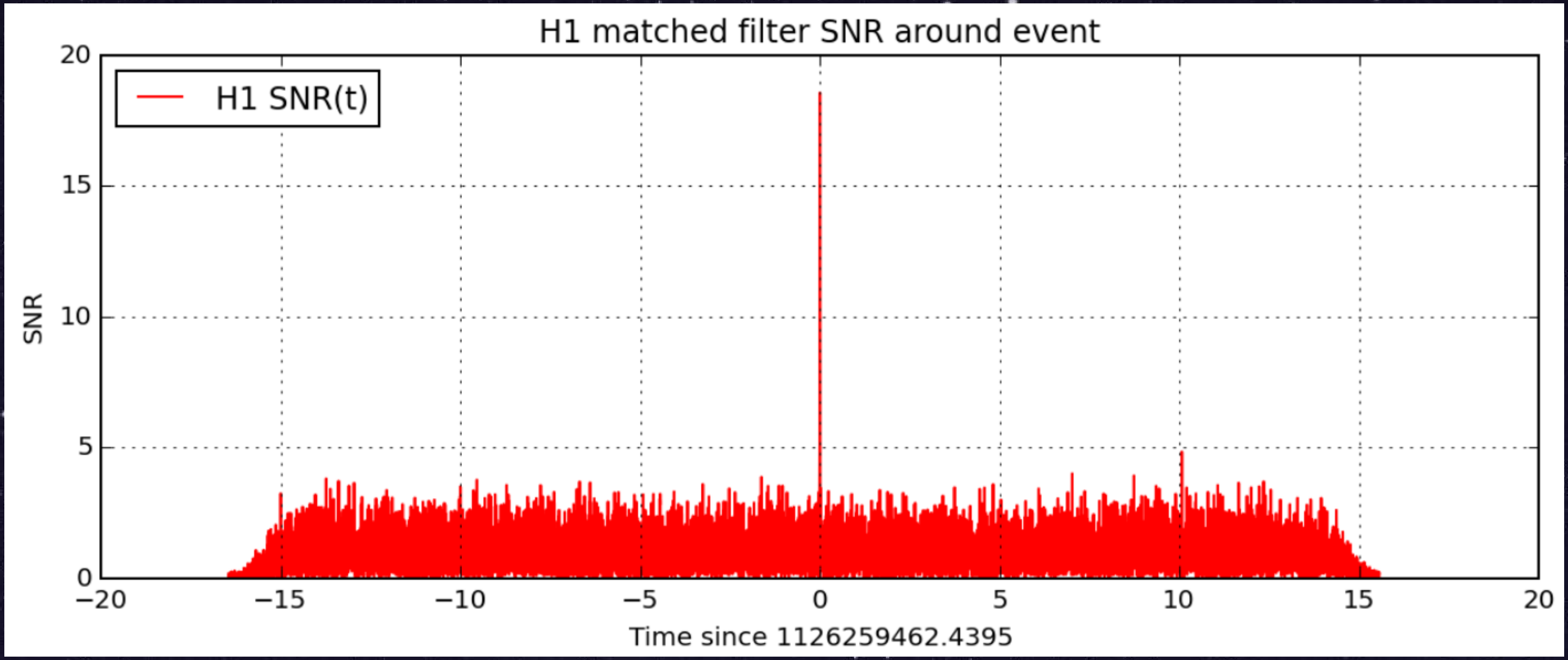

SEOBNRv2 source: https://www.gw-openscience.org

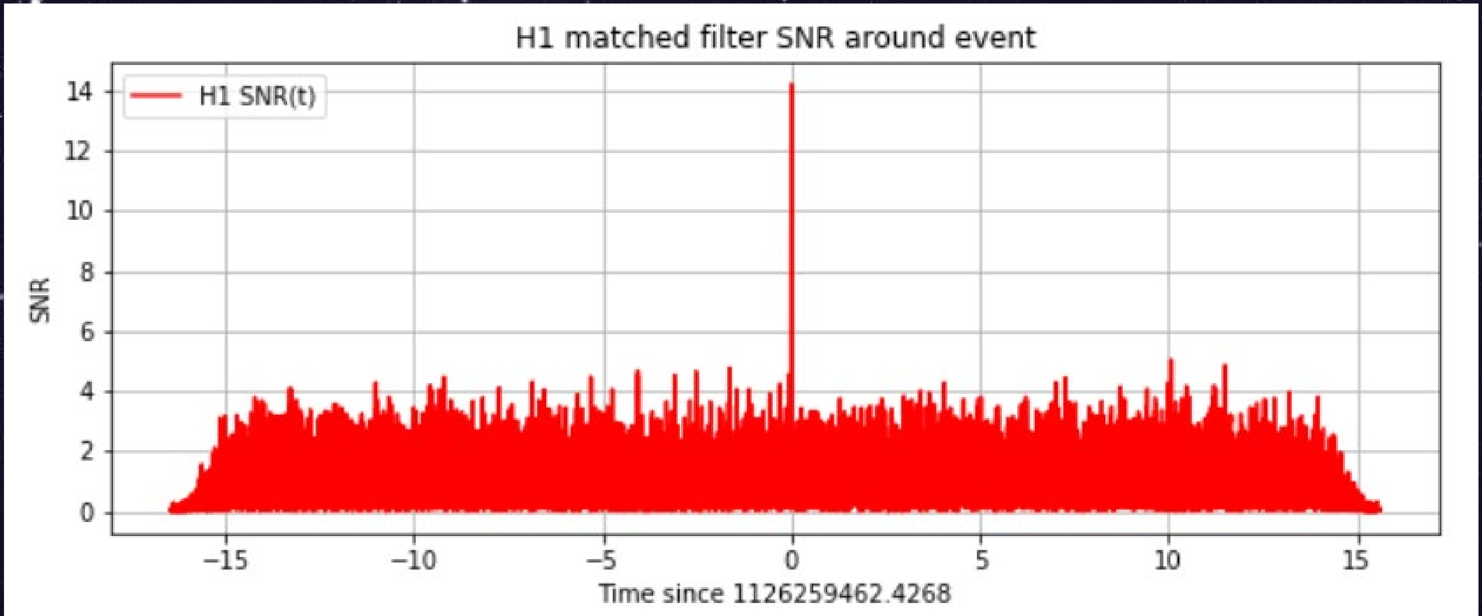

OPN figure courtesy Madhu Jha

Post-Newtonian phase bounds

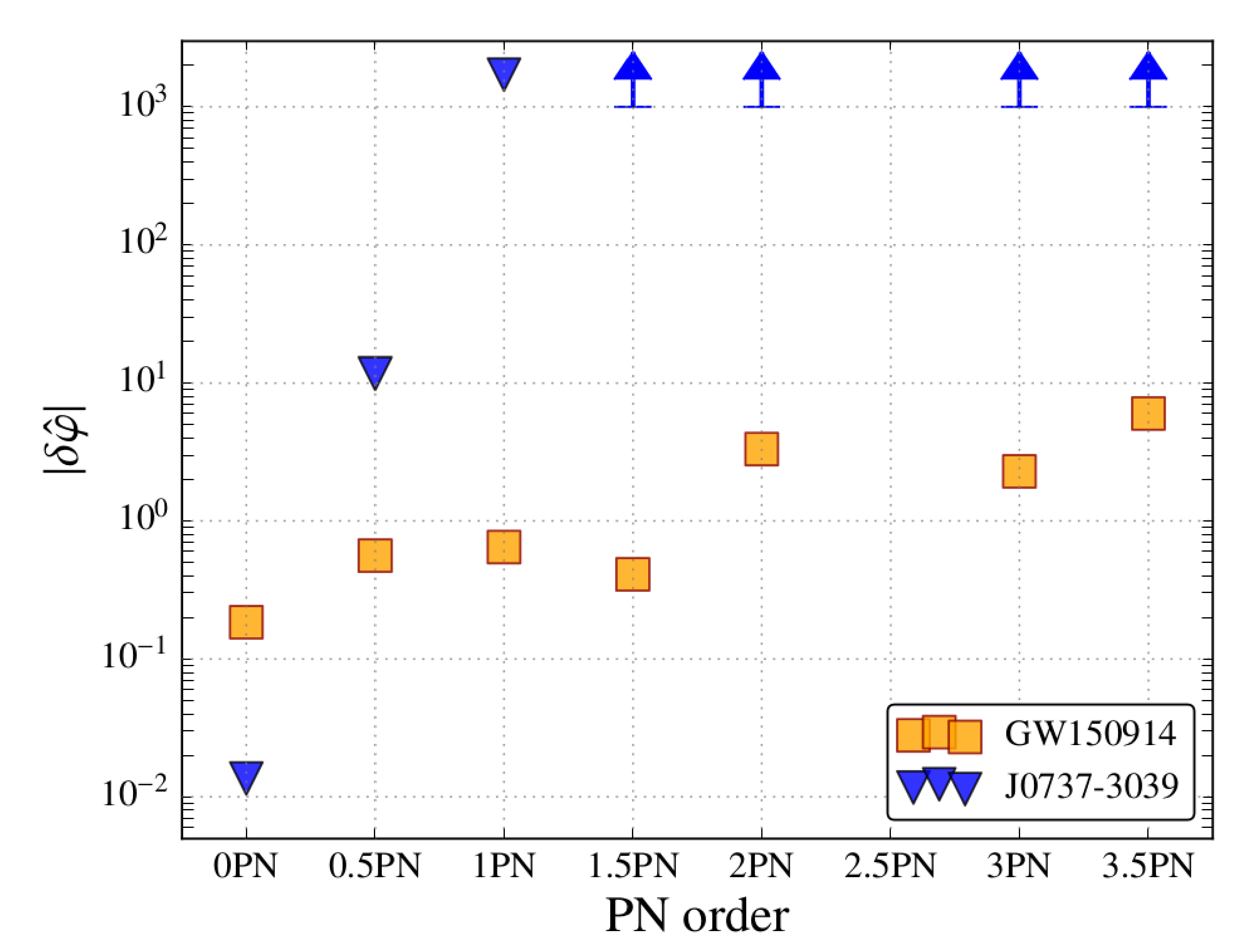

Fig. 6 of LVC PRL 16 (2016) 221101

Theoretical rates: predictions becoming constraints

TABLE II: Compact binary coalescence rates per Milky Way Equivalent Galaxy per Myr.

Source	$R_{\rm low}$	$R_{\rm re}$	$R_{\rm high}$	$R_{\rm max}$
NS-NS ($\rm MWEG^{-1}\ Myr^{-1}$)	1 [1] [a]	100 [1] [b]	1000 [1] [c]	4000 [16] [d]
NS-BH ($\rm MWEG^{-1}\ Myr^{-1}$)	0.05 [18] [e]	3 [18] [f]	100 [18] [g]	
BH-BH ($\rm MWEG^{-1}\ Myr^{-1}$)	0.01 [14] [h]	0.4 [14] [i]	30 [14] [j]	
IMRI into IMBH ($\rm GC^{-1}\ Gyr^{-1}$)			3 [19] [k]	20 [19] [l]
IMBH-IMBH ($\rm GC^{-1}\ Gyr^{-1}$)			0.007 [20] [m]	0.07 [20] [n]

[a] Lower end of 95% confidence interval for the pulsar luminosity distribution yielding the lowest rate (Model 14) in Table 1 of [1]
[b] Peak rate for the reference pulsar luminosity distribution (Model 6) in Table 1 of [1]
[c] Upper end of 95% confidence interval for the pulsar luminosity distribution yielding the highest rate (Model 15) in Table 1 of [1]
[d] Mean rates plus 2σ for Type Ib/Ic supernova [16], values from [17]
[e] The left edge of the probability distribution peak for NS-BH in Figure 6 of [18]
[f] The center of the probability distribution peak for NS-BH in Figure 6 of [18]
[g] The right edge of the probability distribution peak for NS-BH in Figure 6 of [18]
[h] The left edge of the probability distribution peak for BH-BH in Figure 15 of [14]
[i] The center of the probability distribution peak for BH-BH in Figure 15 of [14]
[j] The right edge of the probability distribution peak for BH-BH in Figure 15 of [14]
[k] Estimate from binary hardening via three-body interactions assuming the inspiraling object is a neutron star (Section 2.1 of [19])
[l] Upper limit of $300 M_\odot/m$ per 10^{10} years per cluster (Section 3.3 of [19]), assuming the inspiraling object $m = 1.4\ M_\odot$ is a neutron star
[m] Assumes that 10% of all globular clusters are sufficiently massive and have a sufficient binary fraction to form an IMBH-IMBH binary once in their lifetime, taken to be 13.8 Gyr [20]
[n] Assumes that all globular clusters are sufficiently massive and have a sufficient binary fraction to form an IMBH-IMBH binary once in their lifetime, taken to be 13.8 Gyr [20]

Abadie et al. Class.Quant.Grav 27 173001 (2010)

Data-fitted noise and signal models after O1

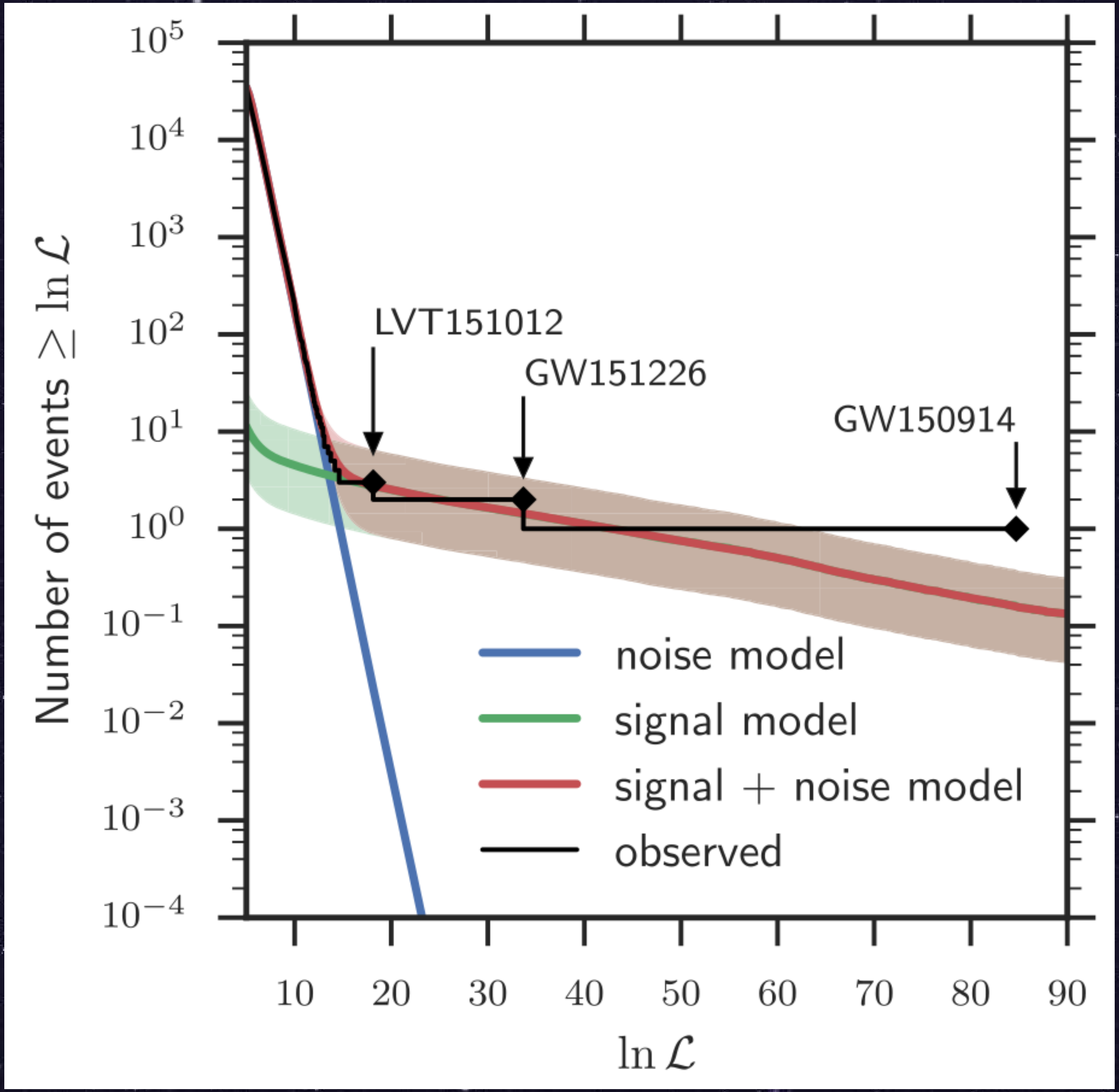

Fig 9 of LVC 1606.04856 PRX6 041015

New signals, 2-OGC catalogue

Date designation	GPS time	$p_{\rm astro}$	FAR^{-1} (y)	Det.	$\tilde{\Lambda}_{\rm BBH}$	ρ_H	ρ_L	ρ_V	$m_1^{\rm src}$	$m_2^{\rm src}$	$\chi_{\rm eff}$	D_L (Mpc)
150914+09:50:45UTC	1126259462.43	> 0.999	> 10000	HL	111.71	19.7	13.4	-	$35.4^{+5.3}_{-3.2}$	$29.8^{+3.1}_{-4.7}$	$-0.04^{+0.11}_{-0.13}$	470^{+140}_{-190}
170814+10:30:43UTC	1186741861.53	> 0.999	> 10000	HL	61.58	9.3	13.8	-	$30.4^{+5.6}_{-2.7}$	$25.8^{+2.6}_{-4}$	$0.08^{+0.12}_{-0.12}$	580^{+130}_{-190}
170823+13:13:58UTC	1187529256.52	> 0.999	> 10000	HL	59.43	6.3	9.2	-	$40^{+11.7}_{-7.1}$	$28.8^{+6.8}_{-7.9}$	$0.05^{+0.21}_{-0.22}$	1750^{+850}_{-820}
170104+10:11:58UTC	1167559936.60	> 0.999	> 10000	HL	47.32	9.1	9.9	-	$31.6^{+7.8}_{-6.3}$	$19.2^{+5}_{-4.1}$	$-0.08^{+0.16}_{-0.18}$	920^{+420}_{-400}
151226+03:38:53UTC	1135136350.65	> 0.999	> 10000	HL	40.58	10.7	7.4	-	$13.9^{+7.9}_{-3.3}$	$7.6^{+2.2}_{-2.3}$	$0.209^{+0.177}_{-0.077}$	460^{+160}_{-180}
151012+09:54:43UTC	1128678900.45	> 0.999	> 10000	HL	20.25	7.0	6.7	-	$22.4^{+13.4}_{-4.8}$	$13.8^{+3.7}_{-4.8}$	$-0.00^{+0.25}_{-0.16}$	990^{+470}_{-460}
170809+08:28:21UTC	1186302519.76	> 0.999	8300[a]	HL	43.34	6.6	10.7	-	$35.2^{+9.5}_{-5.9}$	$23.9^{+5.1}_{-5.3}$	$0.06^{+0.18}_{-0.16}$	980^{+310}_{-390}
170729+18:56:29UTC	1185389807.33	> 0.999	4000	HL	19.16	7.5	7.1	-	55^{+18}_{-13}	32^{+13}_{-10}	$0.31^{+0.22}_{-0.29}$	2300^{+1600}_{-1300}
170608+02:01:16UTC	1180922494.49	> 0.999	> 910	HL	55.12	12.5	8.7	-	$11.6^{+6.7}_{-2.1}$	$7.4^{+1.6}_{-2.3}$	$0.088^{+0.213}_{-0.073}$	310^{+130}_{-110}
170121+21:25:36UTC	1169069154.58	> 0.999	210[a]	HL	23.86	5.1	8.9	-	$33^{+9.2}_{-5.3}$	$25.7^{+5.3}_{-6.1}$	$-0.17^{+0.24}_{-0.26}$	1150^{+950}_{-650}
170818+02:25:09UTC	1187058327.09	> 0.999	5.1[a]	HL	21.42	4.4	9.4	-	$36^{+8.2}_{-5.3}$	$26.2^{+4.8}_{-5.7}$	$-0.11^{+0.20}_{-0.23}$	980^{+430}_{-340}
170727+01:04:30UTC	1185152688.03	0.994	180	HL	15.84	4.5	6.9	-	$41.6^{+12.8}_{-7.9}$	$30.4^{+7.9}_{-8.2}$	$-0.05^{+0.25}_{-0.30}$	2200^{+1500}_{-1100}
170304+16:37:53UTC	1172680691.37	0.70	2.5	HL	11.61	4.6	7.1	-	$44.9^{+17.6}_{-9.4}$	$31.8^{+9.5}_{-11.6}$	$0.11^{+0.29}_{-0.27}$	2300^{+1600}_{-1200}
151205+19:55:25UTC	1133380542.42	0.53	.61	HL	10.97	5.8	4.8	-	67^{+28}_{-17}	42^{+16}_{-19}	$0.14^{+0.40}_{-0.38}$	3000^{+2400}_{-1600}
151217+03:47:49UTC	1134359286.35	0.26	.15	HL	9.61	6.7	5.6	-	46^{+13}_{-26}	$8.2^{+5.1}_{-1.7}$	$0.70^{+0.15}_{-0.50}$	1000^{+660}_{-440}
170201+11:03:12UTC	1169982210.74	0.24	.16	HL	9.26	6.0	5.6	-	48^{+13}_{-23}	$13.1^{+8.6}_{-3.7}$	$0.44^{+0.28}_{-0.54}$	1530^{+1360}_{-770}
170425+05:53:34UTC	1177134832.19	0.21	.2	HL	9.42	5.1	5.8	-	45^{+21}_{-11}	30^{+11}_{-11}	$-0.06^{+0.28}_{-0.32}$	2600^{+2000}_{-1300}
151216+09:24:16UTC	1134293073.19	0.18	.1	HL	9.25	5.9	5.5	-	41^{+15}_{-17}	$14.4^{+7}_{-6.3}$	$0.51^{+0.21}_{-0.57}$	1620^{+1140}_{-910}
170202+13:56:57UTC	1170079035.73	0.13	.06	HL	8.37	5.0	6.6	-	33^{+17}_{-11}	$13.8^{+7}_{-4.8}$	$-0.06^{+0.27}_{-0.32}$	1220^{+980}_{-640}

Table 3 of Nitz et al, arXiv 1910.05331

Binary Neutron Star GW170817

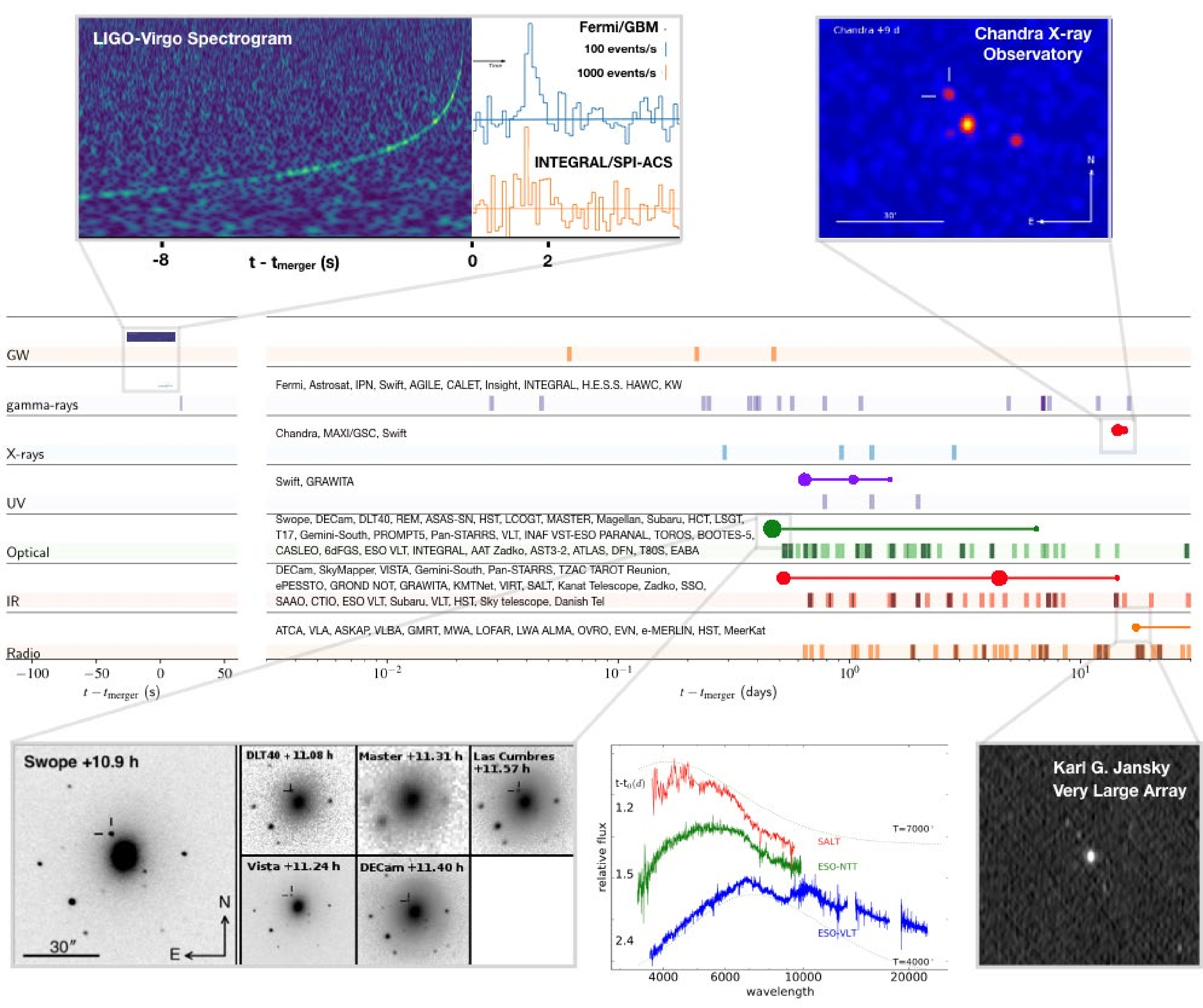

Fig 2, ApJL848, (2017) L12

GW170817 sky location

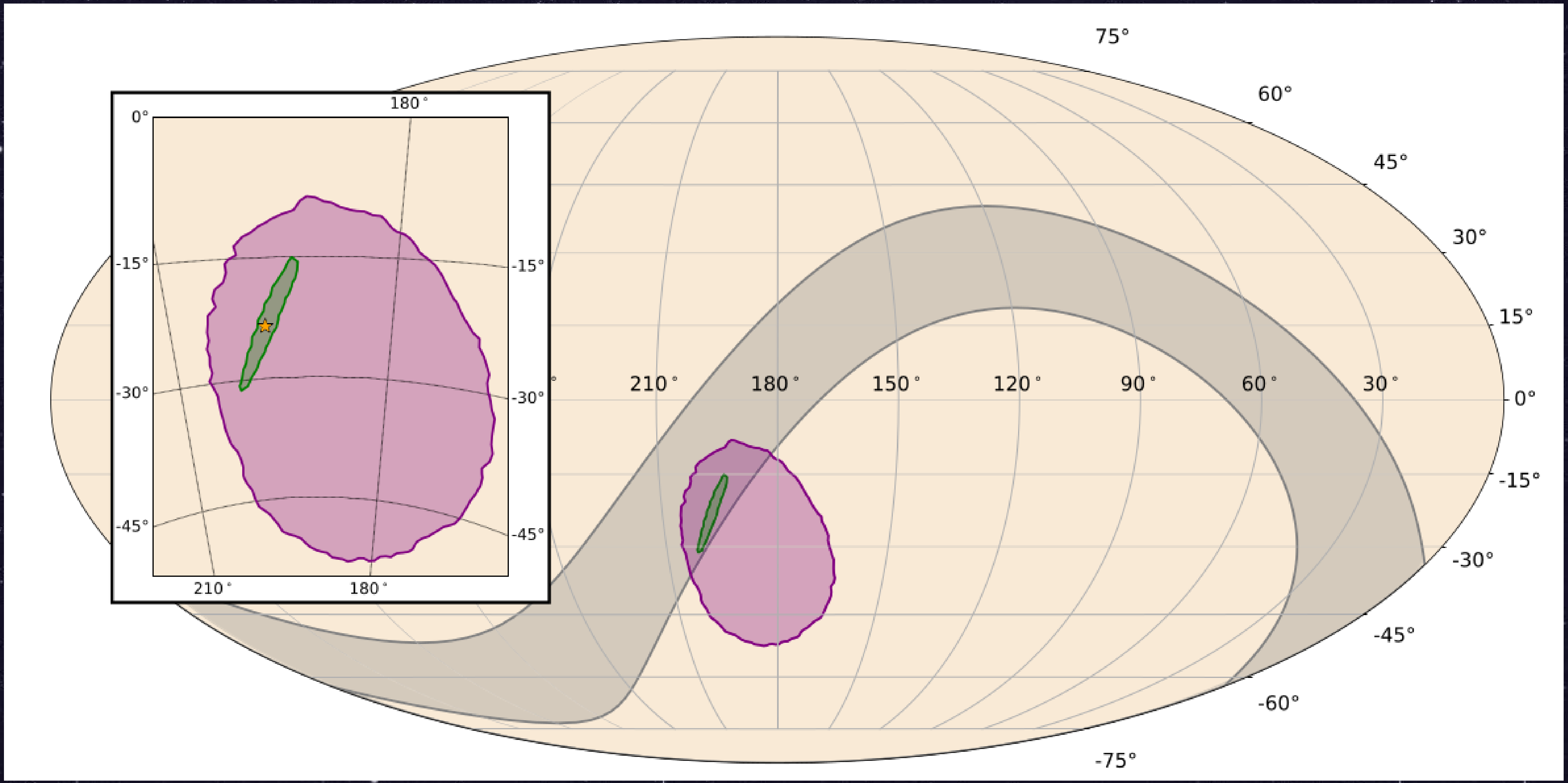

Fig 2, ApJL848, (2017) L13

Binary Neutron Star Merger GW170817

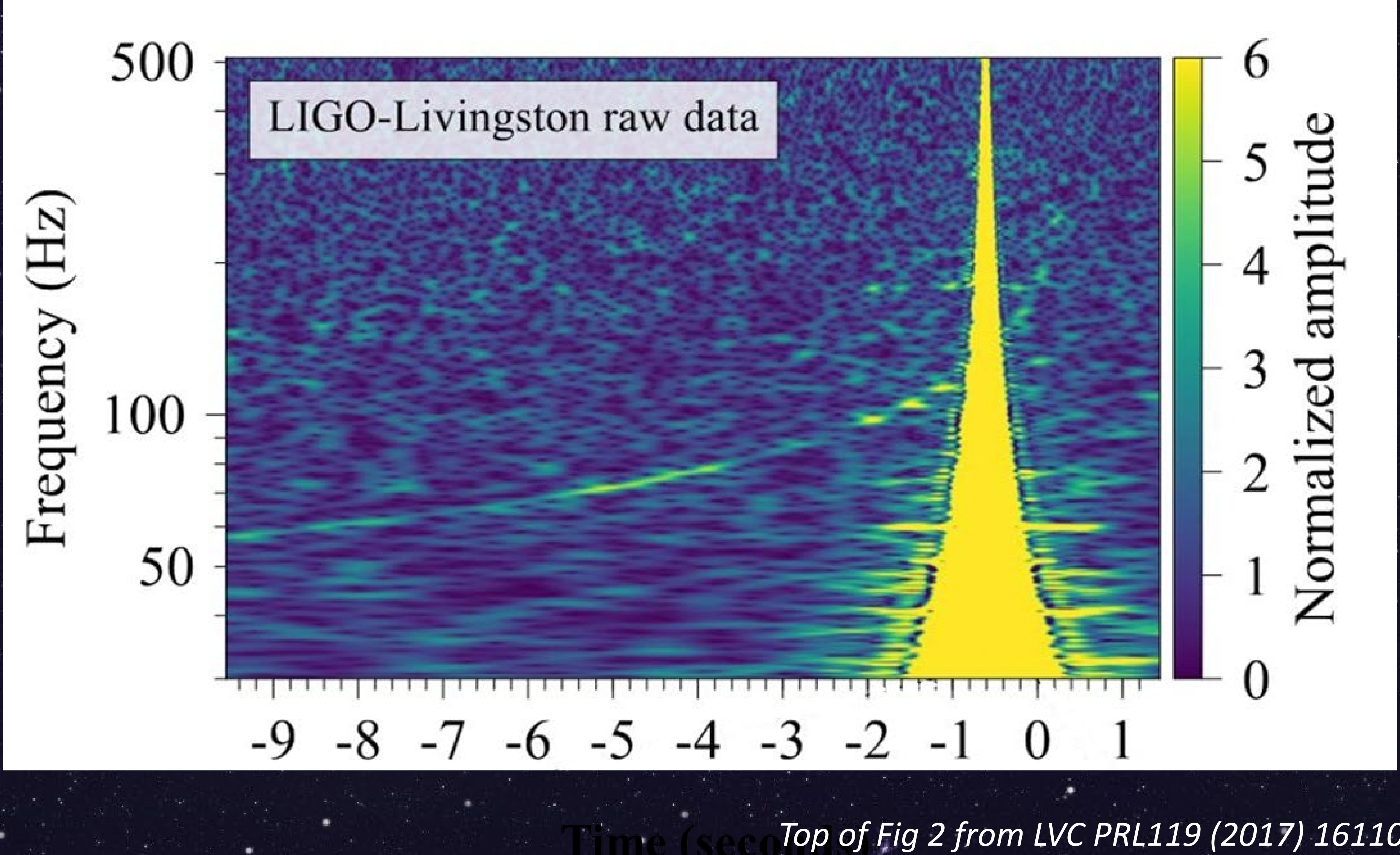

Top of Fig 2 from LVC PRL119 (2017) 161101

BNS, short GRB

- Luminosity distance $\mathbf{40^{+8}_{-14}}$ Mpc, Fermi sGRB 1.7 sec later

- 2010 "realistic" rates projection 1000 per Gpc^3 per year, range 10 to 10,000
- Measured now to be $\mathbf{1540^{+3200}_{-1220}}$ per Gpc^3 per year

- Hubble constant $\mathbf{70^{+12}_{-8}}$ km per second per Mpc

LVC PRL 119 (2017) 161101

- Speed of gravity $\mathbf{-3 \times 10^{-15} \leq \frac{\delta v}{v_{EM}} \leq 7 \times 10^{-16}}$

LVC ApJL 848 (2017) L13

The Origin of the Solar System Elements

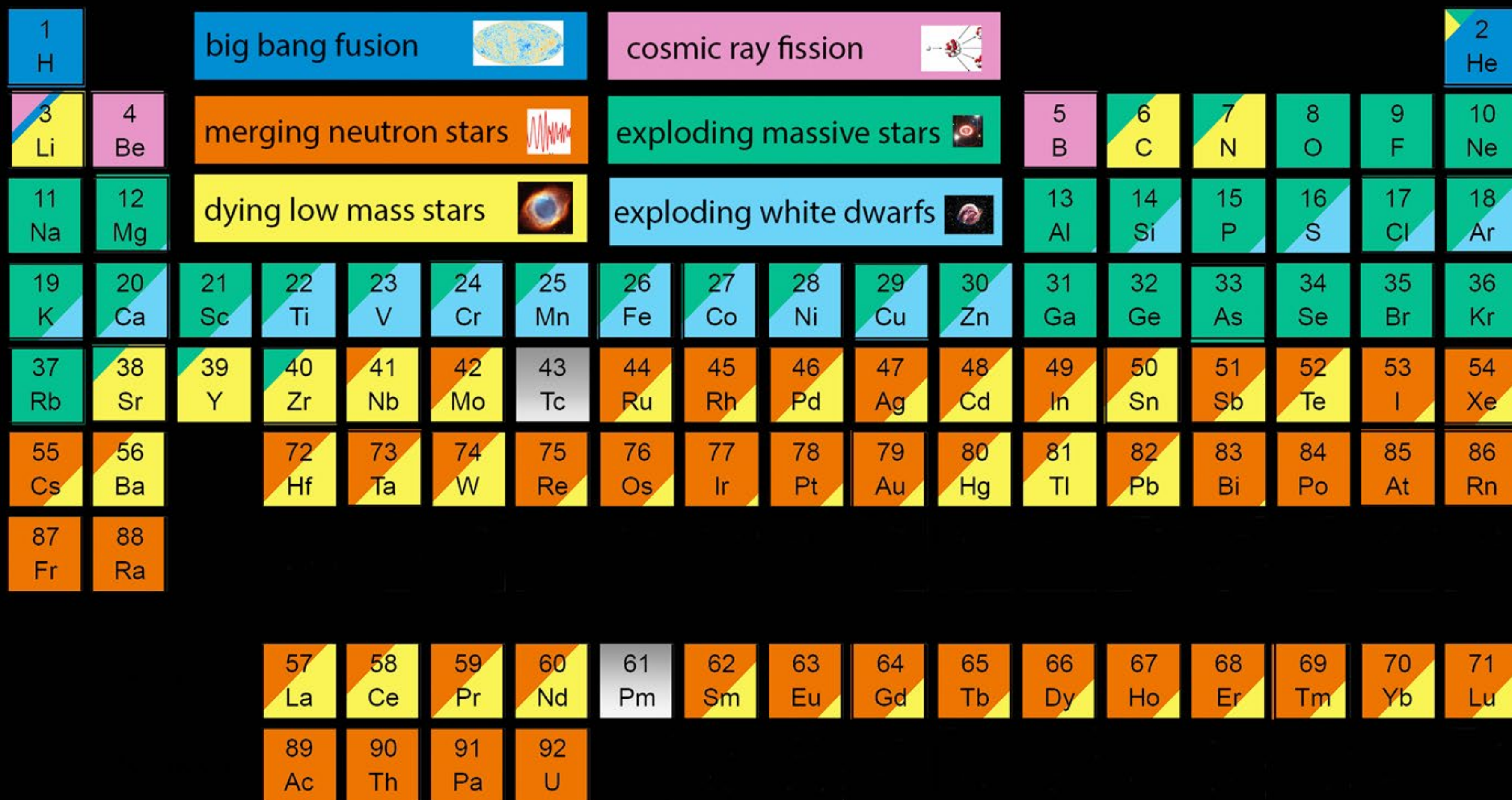

Graphic created by Jennifer Johnson

Astronomical Image Credits:
ESA/NASA/AASNova

Other potential GW sources

- Neutron star – Black hole systems **observed 2019! – awaiting details…**
- Deformed rotating neutron stars
- Galactic supernovae
- Intermediate-mass black holes
- Astrophysical background
- Cosmic strings
- First-order phase transitions
- Inflationary particle production
- Non-perturbative preheating
- Inflationary vacuum fluctuations

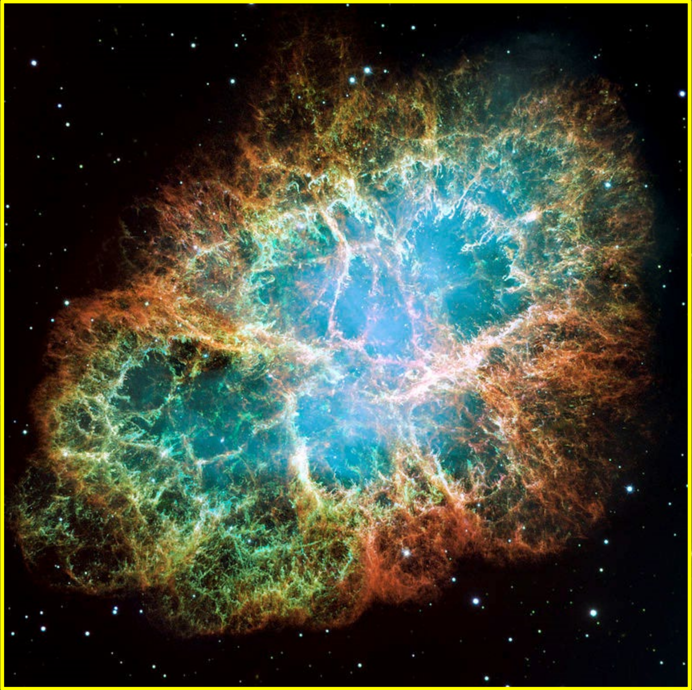

Source: NASA/HST

Worldwide network

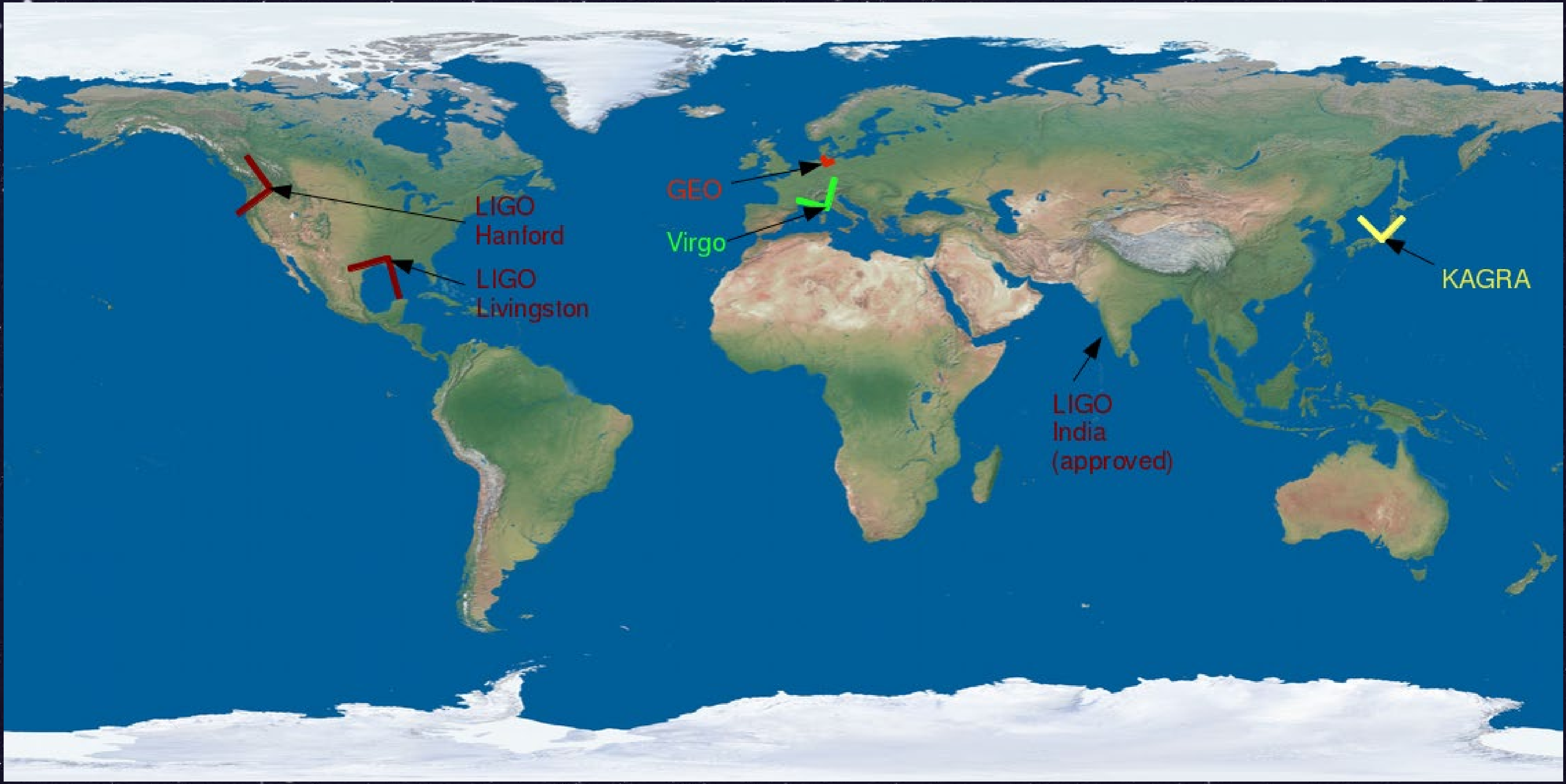

Source: Virgo/LAPP, T. Patterson

Observing scenarios

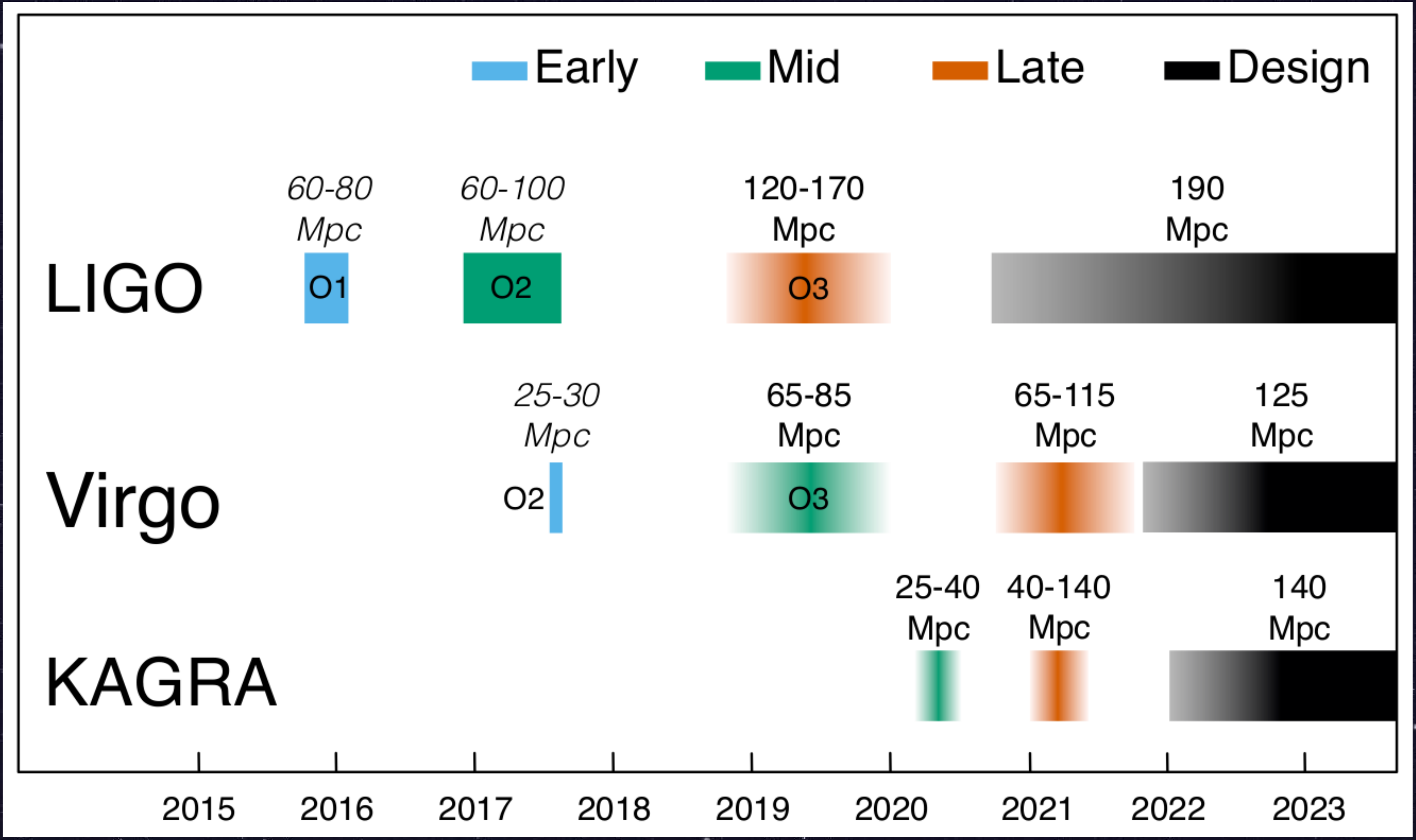

LVC and KAGRA, Fig. 2, Living Rev Relativity (2018) 21: 3

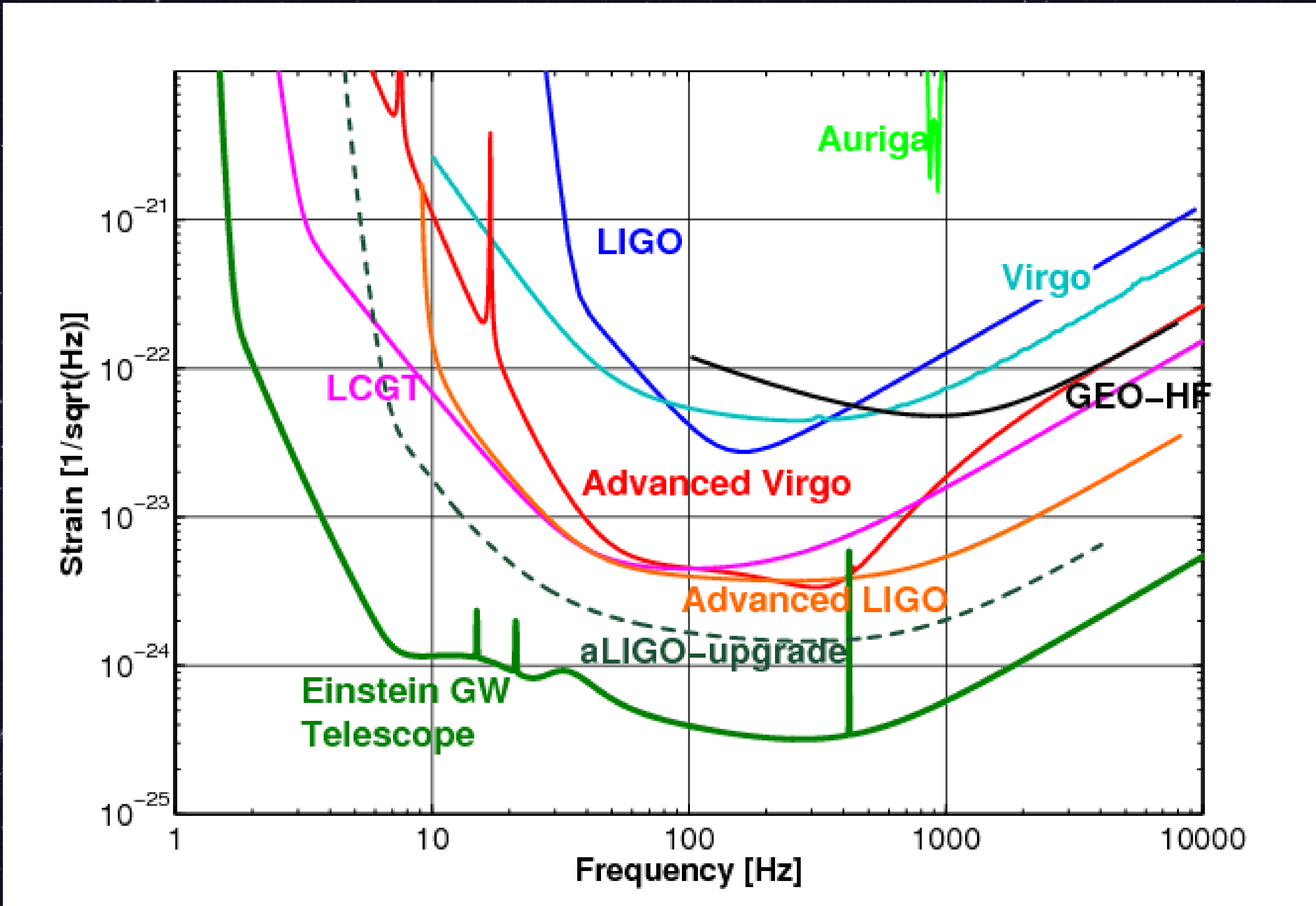

Source: S. Hild (2012)

Full GW spectra

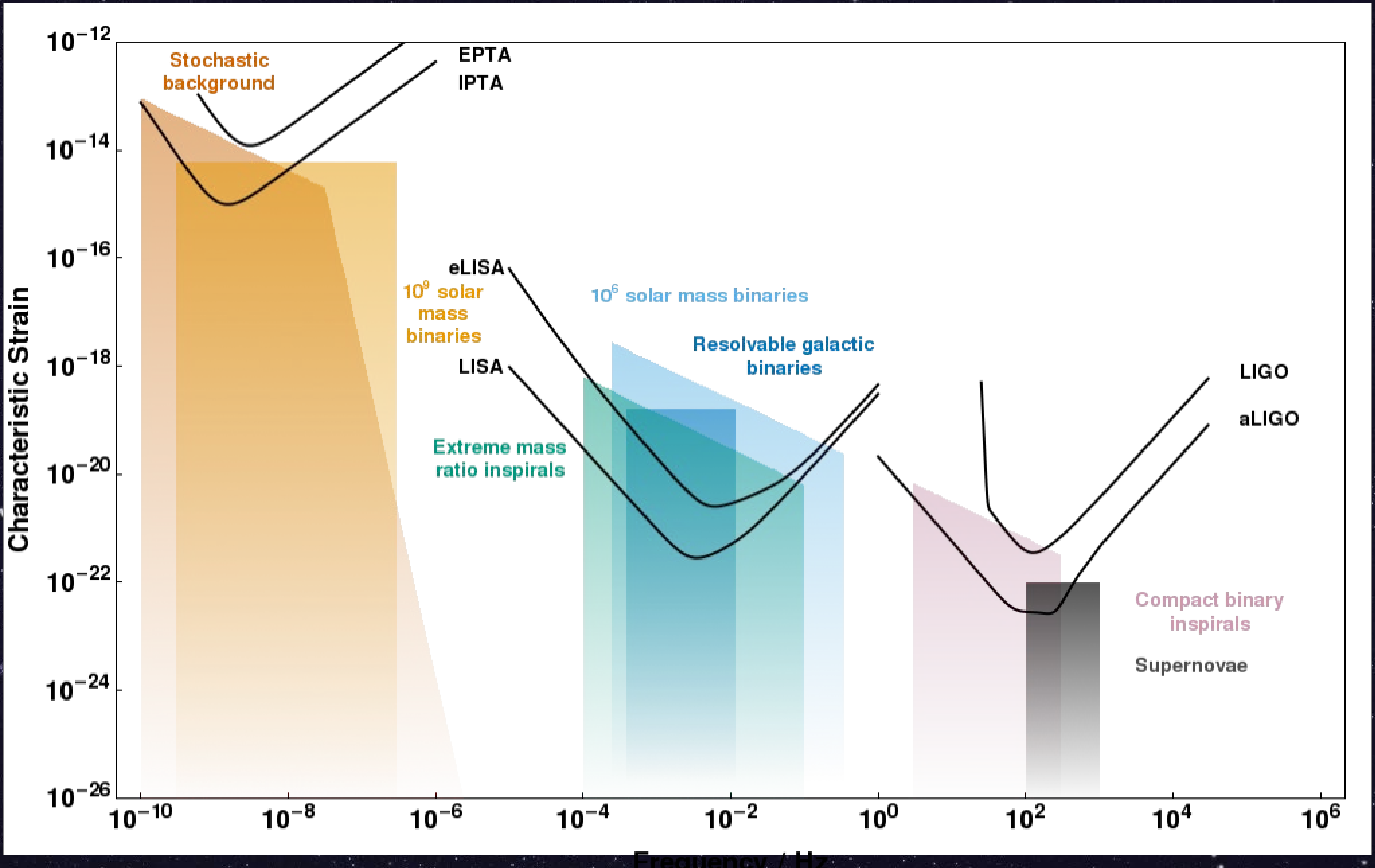

Source: Wikimedia; C. Moore, R. Cole and C. Berry

Reference resources

Abbott et al. *"The basic physics of the binary black hole merger GW150914"* arXiv:1608.01940, Annalen Phys. (2016) 041015

LIGO Open Science Center: https://gw-openscience.org

Science summaries: https://www.ligo.org/science/outreach.php

https://www.zooniverse.org/projects/zooniverse/gravity-spy

Data analysis software: https://wiki.ligo.org/DASWG/LALSuite

Data processing software: https://gwpy.github.io/

Papers: https://www.lsc-group.phys.uwm.edu/ppcomm/Papers.html

PyCBC (Template searches and significance): https://pycbc.org/

cWB (Umodeled search):
https://www.atlas.aei.uni-hannover.de/~waveburst/LSC/doc/cwb/man/

Thank you

Neutron star equation of state

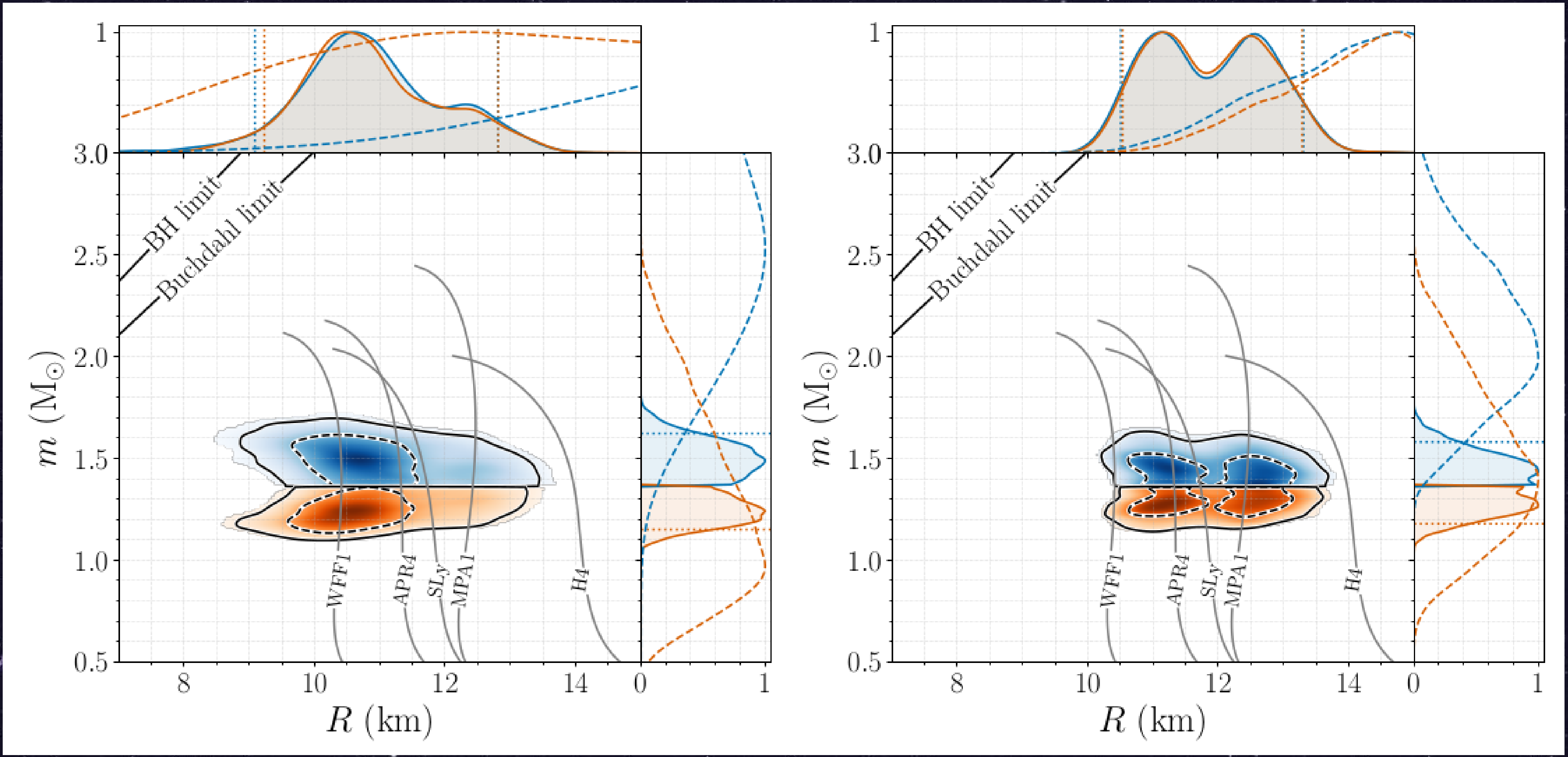

Fig 3 of "*GW170817: Measurements of neutron star radii and equation of state*" LVC arXiv: 1805.11581

FERMI GBM OBSERVATIONS OF LIGO GRAVITATIONAL-WAVE EVENT GW150914

V. Connaughton[1], E. Burns[2], A. Goldstein[3,20], L. Blackburn[4,5], M. S. Briggs[6,7], B.-B. Zhang[7,8], J. Camp[9], N. Christensen[10], C. M. Hui[3], P. Jenke[7] +Show full author list

The Astrophysical Journal Letters, Volume 826, Number 1

Abstract

With an instantaneous view of 70% of the sky, the *Fermi* Gamma-ray Burst Monitor (GBM) is an excellent partner in the search for electromagnetic counterparts to gravitational-wave (GW) events. GBM observations at the time of the Laser Interferometer Gravitational-wave Observatory (LIGO) event GW150914 reveal the presence of a weak transient above 50 keV, 0.4 s after the GW event, with a false-alarm probability of 0.0022 (2.9σ). This weak transient lasting 1 s was not detected by any other instrument and does not appear to be connected with other previously known astrophysical, solar, terrestrial, or magnetospheric activity. Its localization is ill-constrained but consistent with the direction of GW150914. The duration and spectrum of the transient event are consistent with a weak short gamma-ray burst (GRB) arriving at a large angle to the direction in which *Fermi* was pointing where the GBM detector response is not optimal. If the GBM transient is associated with GW150914, then this electromagnetic signal from a stellar mass black hole binary merger is unexpected. We calculate a luminosity in hard X-ray emission between 1 keV and 10 MeV of $1.8^{+1.5}_{-1.0} \times 10^{49}$ erg s^{-1}. Future joint observations of GW events by LIGO/Virgo and *Fermi* GBM could reveal whether the weak transient reported here is a plausible counterpart to GW150914 or a chance coincidence, and will further probe the connection between compact binary mergers and short GRBs.

PHYSICAL REVIEW D
covering particles, fields, gravitation, and cosmology

Wider look at the gravitational-wave transients from GWTC-1 using an unmodeled reconstruction method

F. Salemi, E. Milotti, G. A. Prodi, G. Vedovato, C. Lazzaro, S. Tiwari, S. Vinciguerra, M. Drago, and S. Klimenko

Phys. Rev. D **100**, 042003 – Published 28 August 2019

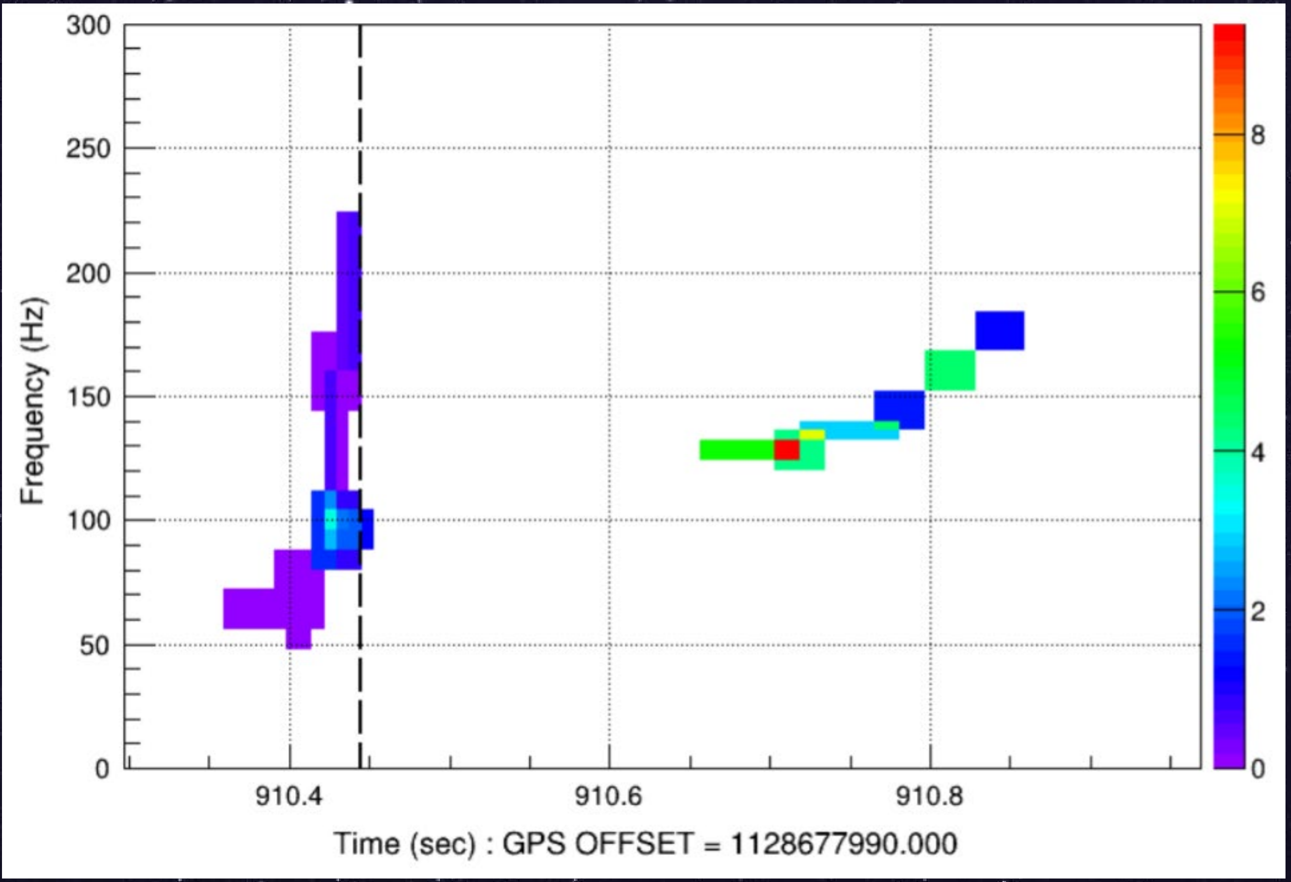

Fig 3d of Salemi et al, PRD100 (2019) 042003

PHYSICAL REVIEW D
covering particles, fields, gravitation, and cosmology

Parameter estimation and statistical significance of echoes following black hole signals in the first Advanced LIGO observing run

Alex B. Nielsen, Collin D. Capano, Ofek Birnholtz, and Julian Westerweck
Phys. Rev. D **99**, 104012 – Published 7 May 2019

Event	Log Bayes factor	Max SNR
GW150914	-1.8056	2.86
LVT151012	1.2499	5.5741
GW151226	0.4186	4.07

TABLE II. Table of Bayes factor results. Negative values indicate that the Gaussian noise hypothesis is preferred. Positive values indicate that the echoes hypothesis is preferred after marginalization over parameters. Log Bayes values with magnitude < 1 are "not worth more than a bare mention" in the nomenclature of [43].

Table II of Nielsen et al, PRD99 (2019) 104012

X-ray binaries masses and spin

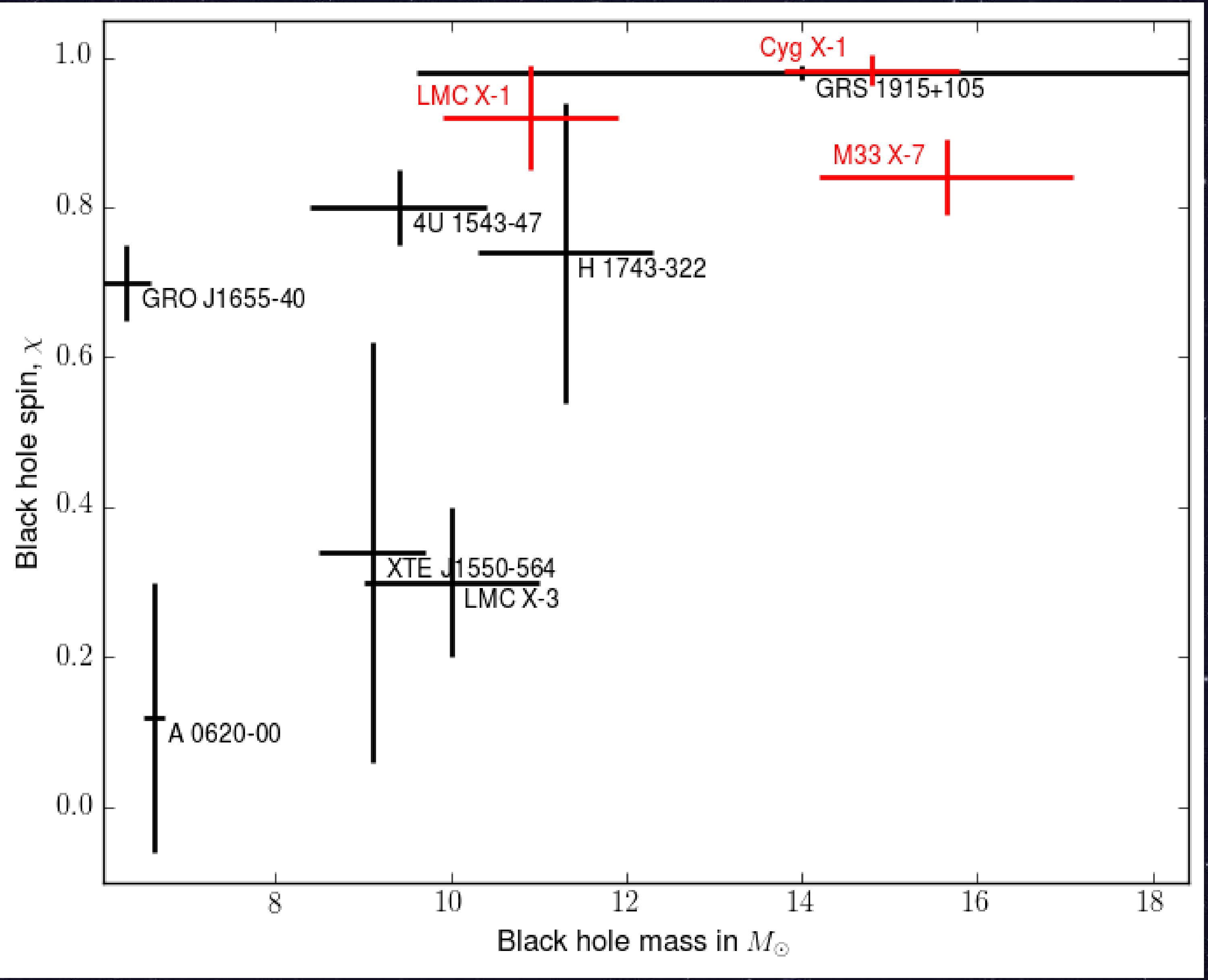

Fig. 1 of Nielsen J.Phys.Conf.Ser. 716 (2016) no.1, 012002

X-ray + GW masses and spins

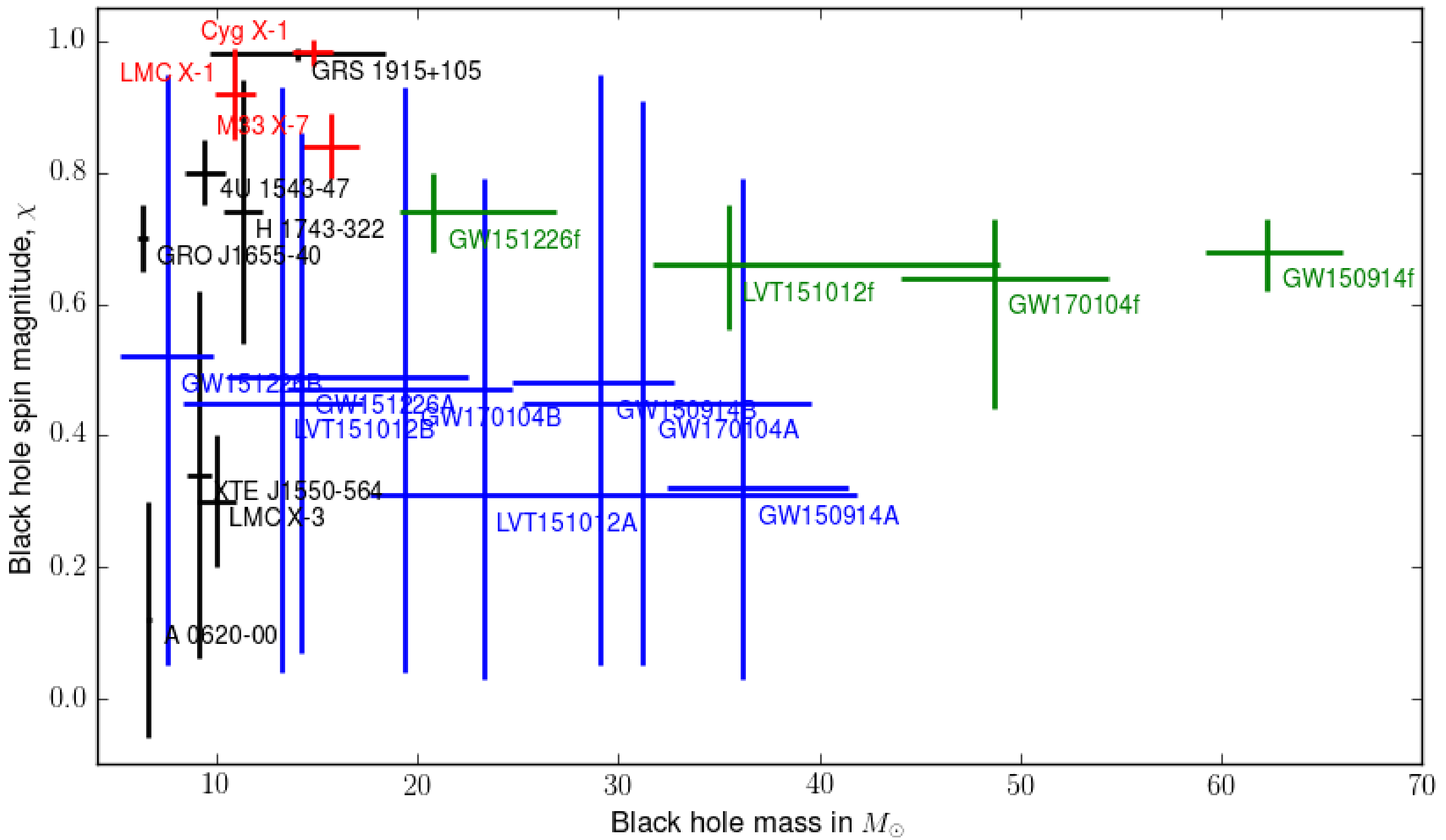

THE GRAVITATIONAL WAVE SPECTRUM

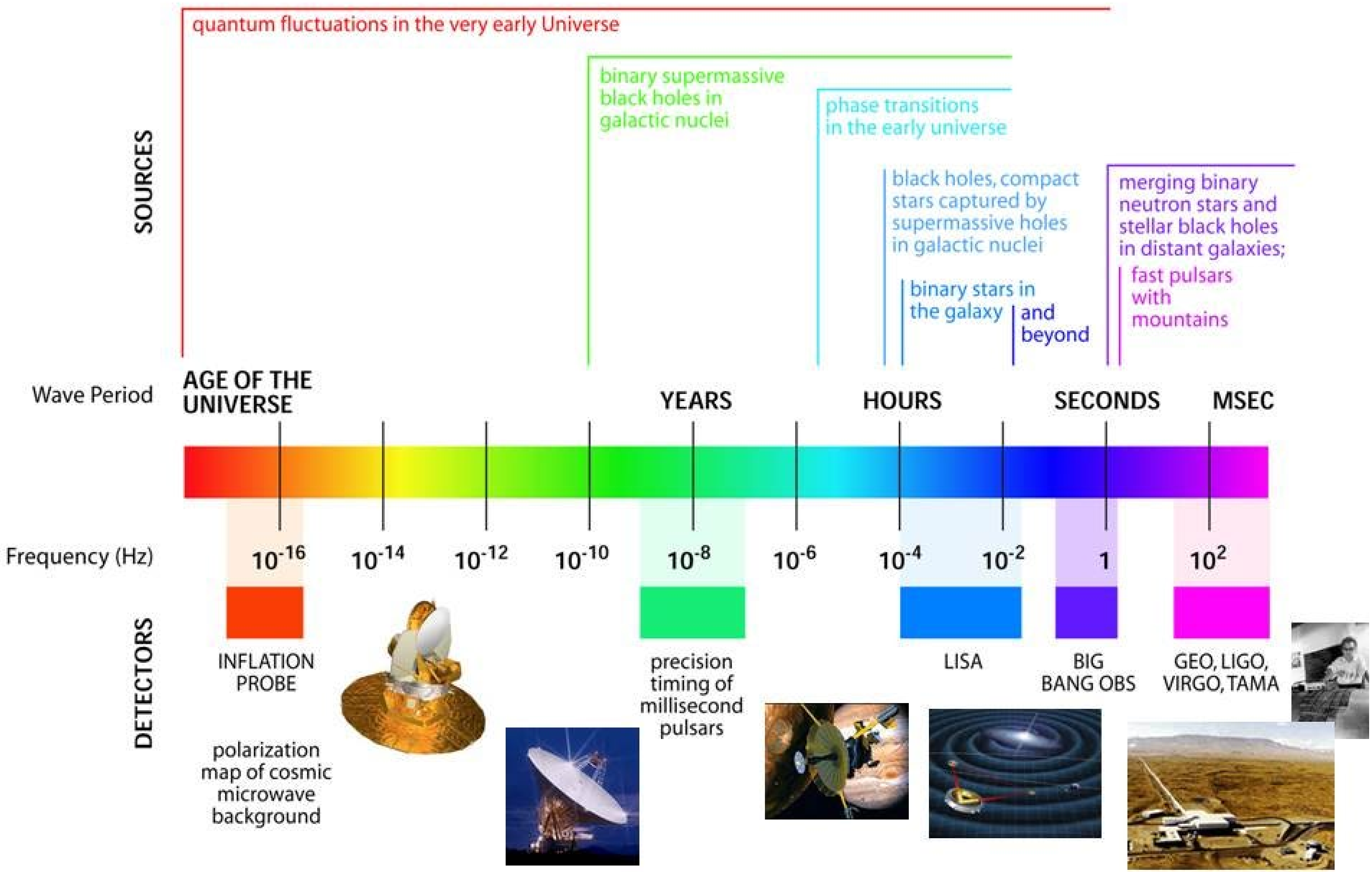

Source: Martin Hendry